NAVAL POSTGRADUATE SCHOOL

MONTEREY, CALIFORNIA

THESIS

THE EFFECTS OF A REMOTE ATOLL AND LAGOON ON THE MARINE BOUNDARY LAYER

by

Eric L. Daley

December 2012

Thesis Advisor: Qing Wang
Second Reader: Wendell Nuss

Approved for public release; distribution is unlimited

THIS PAGE INTENTIONALLY LEFT BLANK

REPORT DOCUMENTATION PAGE			Form Approved OMB No. 0704-0188
Public reporting burden for this collection of information is estimated to average 1 hour per response, including the time for reviewing instruction, searching existing data sources, gathering and maintaining the data needed, and completing and reviewing the collection of information. Send comments regarding this burden estimate or any other aspect of this collection of information, including suggestions for reducing this burden, to Washington headquarters Services, Directorate for Information Operations and Reports, 1215 Jefferson Davis Highway, Suite 1204, Arlington, VA 22202-4302, and to the Office of Management and Budget, Paperwork Reduction Project (0704-0188) Washington DC 20503.			
1. AGENCY USE ONLY *(Leave blank)*	**2. REPORT DATE** December 2012	**3. REPORT TYPE AND DATES COVERED** Master's Thesis	
4. TITLE AND SUBTITLE The Effects of a Remote Atoll and Lagoon on the Marine Boundary Layer		**5. FUNDING NUMBERS**	
6. AUTHOR(S) Eric L. Daley			
7. PERFORMING ORGANIZATION NAME(S) AND ADDRESS(ES) Naval Postgraduate School Monterey, CA 93943-5000		**8. PERFORMING ORGANIZATION REPORT NUMBER**	
9. SPONSORING /MONITORING AGENCY NAME(S) AND ADDRESS(ES) N/A		**10. SPONSORING/MONITORING AGENCY REPORT NUMBER**	
11. SUPPLEMENTARY NOTES The views expressed in this thesis are those of the author and do not reflect the official policy or position of the Department of Defense or the U.S. Government. IRB Protocol number _____N/A_____.			
12a. DISTRIBUTION / AVAILABILITY STATEMENT Approved for public release; distribution is unlimited		**12b. DISTRIBUTION CODE**	

13. ABSTRACT (maximum 200 words)

The presence of an island is known to affect the marine environment in multiple ways depending on the size, shape, and particularly the topography of the island. The dominant effect is seen in the atmospheric boundary layer through the significant change in surface roughness and land surface heating, while steep topography on a small island may affect large scale systems such as tropical cyclones. In this study, we investigate the role of a small remote coral atoll, Diego Garcia, in the Indian Ocean in modifying the marine environment. Dropsonde measurements made near the island were used to identify the effects of Diego Garcia in wind reduction and moisture enhancement. A case analysis was made using measurements from 04 December 2011 to quantify horizontal and vertical extent and the magnitude of the effects. Additionally, high-resolution COAMPS simulations were used to examine the potential of using mesoscale model to quantify flow modifications by small islands. COAMPS was able to simulate the wind reduction by the island, but could not quantify its effect on low-level moisture. Finally, a comparison between the dropsonde nearby and rawinsonde measurements from the island reveals the deficiency of the island-based rawinsonde measurements in representing the marine environment.

14. SUBJECT TERMS Madden-Julian Oscillation (MJO), Dynamics of the Madden-Julian Oscillation (DYNAMO), Dropsonde			**15. NUMBER OF PAGES** 77
			16. PRICE CODE
17. SECURITY CLASSIFICATION OF REPORT Unclassified	**18. SECURITY CLASSIFICATION OF THIS PAGE** Unclassified	**19. SECURITY CLASSIFICATION OF ABSTRACT** Unclassified	**20. LIMITATION OF ABSTRACT** UU

NSN 7540-01-280-5500

Standard Form 298 (Rev. 2-89)
Prescribed by ANSI Std. 239-18

THIS PAGE INTENTIONALLY LEFT BLANK

Approved for public release; distribution is unlimited

THE EFFECTS OF A REMOTE ATOLL AND LAGOON ON THE MARINE BOUNDARY LAYER

Eric L. Daley
Lieutenant Commander, United States Navy
B.S., University of South Carolina, 2003

Submitted in partial fulfillment of the
requirements for the degree of

MASTER OF SCIENCE IN METEOROLOGY AND PHYSICAL OCEANOGRAPHY

from the

NAVAL POSTGRADUATE SCHOOL
December 2012

Author: Eric L. Daley

Approved by: Dr. Qing Wang
Thesis Advisor

Second Reader
Wendell Nuss

Dr. Wendell A. Nuss
Chair, Department of Meteorology

THIS PAGE INTENTIONALLY LEFT BLANK

ABSTRACT

The presence of an island is known to affect the marine environment in multiple ways depending on the size, shape, and particularly the topography of the island. The dominant effect is seen in the atmospheric boundary layer through the significant change in surface roughness and land surface heating, while steep topography on a small island may affect large scale systems such as tropical cyclones. In this study, we investigate the role of a small remote coral atoll, Diego Garcia, in the Indian Ocean in modifying the marine environment. Dropsonde measurements made near the island were used to identify the effects of Diego Garcia in wind reduction and moisture enhancement. A case analysis was made using measurements from 04 December 2011 to quantify horizontal and vertical extent and the magnitude of the effects. Additionally, high-resolution COAMPS simulations were used to examine the potential of using mesoscale model to quantify flow modifications by small islands. COAMPS was able to simulate the wind reduction by the island, but could not quantify its effect on low-level moisture. Finally, a comparison between the dropsonde nearby and rawinsonde measurements from the island reveals the deficiency of the island-based rawinsonde measurements in representing the marine environment.

THIS PAGE INTENTIONALLY LEFT BLANK

TABLE OF CONTENTS

THIS PAGE INTENTIONALLY LEFT BLANK

LIST OF FIGURES

THIS PAGE INTENTIONALLY LEFT BLANK

LIST OF TABLES

THIS PAGE INTENTIONALLY LEFT BLANK

LIST OF ACRONYMS AND ABBREVIATIONS

ARM	Atmospheric Radiation Measurement
BIOT	British Indian Ocean Territory
C	Celsius
CINDY2011	Cooperative Indian Ocean Experiment on Intraseasonal Variability in Year 2011
COAMPS	Coupled Ocean Atmospheric Mesoscale Prediction System
DOE	Department of Energy
DYNAMO	Dynamics of Madden-Julian Oscillation
EOP	Extended Observation Period
GMS	Global Positioning System
hPa	hectopascals
IBL	Internal Boundary Layer
IOP	Intensive Observation Period
MATLAB	Matrix Laboratory
mb	millibars
MBL	Marine Boundary Layer
MJO	Madden-Julian Oscillation
NMOC	Navy Meteorology and Oceanography Command
NOAA	National Oceanographic and Atmospheric Administration
NOGAPS	Navy Operational Global Atmospheric Predictive System
NPS	Naval Postgraduate School
PTH	Pressure, Temperature, and Humidity
RBS	Reigal scanning surface wave lidar Bore Siting

SOP	Special Observation Period
SST	Sea Surface Temperature
TC	Tropical Cyclone
TIBL	Thermal Internal Boundary Layer
TKE	Turbulent Kinetic Energy
TWP	tropical Western Pacific Ocean
UHI	Urban Heat Island

ACKNOWLEDGMENTS

I would like to express my appreciation to Professor Qing Wang for your help and support throughout this process. I want to thank you for your guidance and vast knowledge regarding boundary layer processes and your MATLAB expertise. It was a privilege to work with you. I would also like to thank the following people who have contributed significantly to the completion of this work and my success as a student at NPS:

- The NOAA WP-3D Orion (Miss Piggy) flight crew for making this research possible and the NCAR dropsonde data quality control personnel.
- June Wang and Kate Young for dropsonde data processing and quality control.
- Hway-Jen Chen, for COAMPS simulations and analyses.
- Mike Cook, for the varied and extensive MATLAB assistance and teaching.
- Kurt Nielsen, for satellite data support.

I would like to thank the following individuals who through the years are directly responsible for my success and deserve the credit for where I stand today and what I have accomplished: The Lord Jesus Christ, Petty Officer Kevin Davis, Chief Petty Officers Bentley, Sanderson and Moffitt, Commander Barry Bakos, Dr. Greg Carbone and Dr. Susan Cutter, both of the University of South Carolina.

I would like to dedicate this work to my wife: Maran. Your love and patience have greatly helped me through this research. Your unyielding support and untiring devotion to me and our children will always be appreciated. Thank you!

THIS PAGE INTENTIONALLY LEFT BLANK

I. INTRODUCTION

A. MILITARY SIGNIFICANCE AND MOTIVATIONS

1. Accurate Forecasting For Data Sparse Regions

In recent years the funding constraints and capabilities of military weather forecasting have led to reorganization and restructuring of how meteorological, oceanographic, and other geophysical intelligence and mission specific products are generated and delivered. The major change was a geographic reorganizing of forecasting commands and production centers in functional commands. The Naval Meteorology and Oceanography Command (NMOC) shifted from a regional support structure to a mission specific support structure. These changes along with reduced manning led to meteorological and oceanographic forecasting and tailored product support being centrally produced and delivered to military customers electronically. This means that the forecaster is no longer travelling with the military unit and directly capable of obtaining or supervising observations for forecasting purposes. Reliance on the internet and other electronic communications to obtain in-situ data of nearby sensors for use in the forecasting process has always been done but now the forecaster is not present and cannot obtain or verify the observations for the forecast location. The in-situ data is invaluable for determining current conditions, validating model accuracy, and verifying previous forecasts. When military units operate far from established meteorological sensing networks, especially far from continental shores, forecasters rely on models and use the nearest in-situ and most recent satellite observations to check model performance and produce the forecast. The use of a surface observation from a remote island is a common if not required step in the forecast process for support to military units far from shore and established sensing networks. Unless the islands impacts on the boundary layer and atmospheric processes is known the observed measurements can be used in error and accurate model prediction can be disregarded or vise-versa, leading to reduced forecast accuracy and potentially adverse mission impacts.

2. Strategic Importance of the Indian Ocean

The Indian Ocean's importance to U.S. foreign policy and military power projection is well known as it is adjacent to four key areas: the Middle East, Central and South Asia, and the Asia-Pacific region. Furthermore, the Indian Ocean is a major goods and energy transit route, the location of much of the prepositioned military assets, the site of key inflection points, and multiple potential hotspots. As stated in recent Quadrennial Defense Review, National Security Strategy, and Unified Command Plan, the strategic importance of the Indian Ocean is at the forefront of U.S. policy and is expected to grow significantly in the future (Erickson et al. 2010). The Indian Ocean is also a data sparse region, making the few temporally consistent in-situ observations, such as those from Diego Garcia surface and upper air, invaluable. Understanding of how the surface and upper-air in-situ measurements on or near islands are impacted by the presence of the island is critical for accurate forecasting and model performance. An understanding of the impacts and limitations of in-situ observations from remote islands will improve forecasts and increase mission effectiveness, efficiency, and battle force safety.

B. THESIS OBJECTIVES

This work focuses on the modification of the Marine Boundary Layer (MBL) by a small island, Diego Garcia. Primary questions center on what the island and lagoon's presence has on low level wind, temperature and humidity, to what geographic extent the effects can be found, the variability of the effects, whether or not the presence and distribution of clouds are impacted, how to understand the larger marine environment from in-situ surface and upper air observations, and if high-resolution models are able to accurately account for the effects. By identifying the geographic extent and magnitude that Diego Garcia and the lagoon has on the MBL, forecasters and modelers can determine the true conditions for a broader region and improve model skill and forecast accuracy. These objectives are met by using mainly dropsonde measurements, augmented by rawinsonde, and aircraft based measurements during the Dynamics of the Madden-Julian Oscillation (DYNAMO) field campaign. Dropsonde and aircraft measurements was based on a research aircraft operated by the National Atmospheric and Oceanographic Administration (NOAA), a WP-3D "Miss Piggy" (hereafter the P-3) and

is depicted in Fig. 1. This observational study was further augmented with simulations using high-resolution Coupled Ocean Atmosphere Mesoscale Prediction System (COAMPS) model.

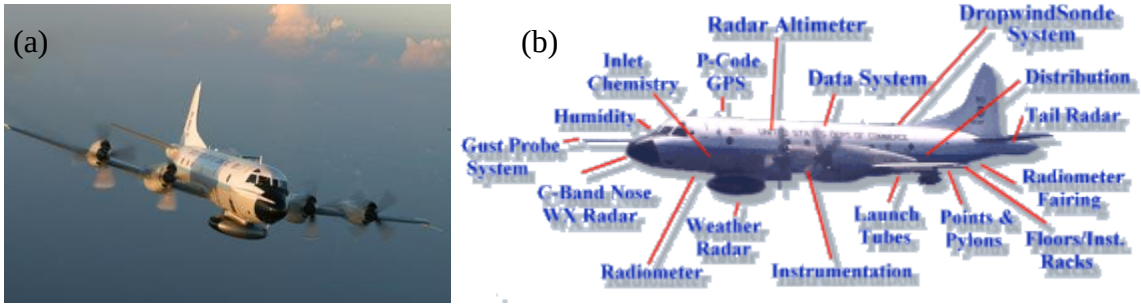

Figure 1. (a) A photograph of the P-3 in flight; (b) an image of the P-3 Orion aircraft built by Lockheed with some of the main atmospheric sensing instruments labeled and their locations identified. Both images are from the NOAA web site, 2012 (Images from NOAA, http://www.aoc.noaa.gov/).

C. SCOPE OF RESEARCH

This thesis achieves research goals through the analysis of data obtained from research flights associated with the DYNAMO project that was conducted in November and December of 2011. The intensive Observation Period of DYNAMO was conducted in a region from 8°S to 0.3°N latitude and 70.9°E to 80.5°E longitude. A total of 468 dropsondes were deployed with 47 dropped within a 100 km radius of Diego Garcia. Important variables used from the DYNAMO P-3 flights include the wind speed, wind direction, specific humidity, relative humidity, potential temperature, vertical velocity, and sea surface temperature (SST) data from on board instruments. With the exception of SST and vertical velocity, the same meteorological data was collected from the dropsonde's that were launched by the P-3 within 100 km of the island and the island-based rawinsondes. High-resolution simulations of COAMPS was also used to examine the effects Diego Garcia and the lagoon have on the MBL and limitations identified regarding the models forecast of the MBL near the island.

This thesis will investigate the low-level vertical profiles of wind, temperature, and water vapor from soundings made close to the island and identify various

atmospheric layers, their specific structures, and determine how the MBL was affected by the presence of the island. Statistical analyses and various graphic presentations will be used to quantify the island effects by comparing soundings close to the island and those from the open marine environment. This thesis will also compare temporally coincident balloon rawinsonde soundings from the island to those from nearby dropsondes to illustrate the limitations of a rawinsonde launched from the small island in representing marine environment. The key steps to be taken in this research project are identifying the land and water characteristics of Diego Garcia, dropsonde data processing, and analyses of meteorological parameters in light of the in-situ measurement's location relative to Diego Garcia. Further steps include analyses of aircraft based measurements, categorizing low-level layer structures for soundings close to Diego Garcia according to wind direction, temperature, and water vapor. A case analysis for upwind and downwind dropsonde profiles was made to identify island effects, comparison of dropsondes with the island launched upsondes, and identification of upsondes limitations in representing the marine environment.

II. BACKGROUND

A. THE INTERNAL BOUNDARY LAYERS

The Internal Boundary Layer (IBL) is defined as air that is modified by flow over a surface of different characteristics (Stull 1988). Since the new boundary layer is within an existing layer the term internal is added to denote the change in surface conditions and its effect on the new "internal" boundary layer. In the situation where atmospheric flow is from a smooth to a rougher surface the air will slow down leading to horizontal convergence and upward motion. The reverse is true as flow from rough to smooth will experience divergence at the surface and descending air. In the latter case, frictional velocity decreases and turbulent kinetic energy (TKE) increases slightly at the border between smooth and rough surfaces. The IBL grows downwind by entrainment and can be capped by an inversion or upper level subsistence. With all of the changes associated with the new IBL the total effect will ultimately reach a new equilibrium level at some distance downwind of the border between the surfaces. A specific type of IBL, the thermal internal boundary layers (TIBLs), is one example of many possible air mass modifications. Should the surface change across a boundary include heat flux in addition to a roughness change, the IBL is further modified as a result of heat flux difference. Conceptual illustrations of and IBL and TIBL are pictured in Fig. 2. A TIBL is found when the surface has differing albedos, temperatures, or emissivities. A specific TIBL is the convective TIBL that develops when the flow is from a cooler surface to a warmer surface such as from ice pack to an adjacent liquid water body. In Fig. 2a, it is seen that the TIBL extends further downwind from the surface property change. When the flow is from warmer to cooler surfaces a stable TIBL develops that experiences a marked decay in turbulence from the increased static stability. Some turbulence remains and is generated by shear near the surface or adjacent air masses. Convective TIBLs have well defined mixed layer top while stable TIBLs do not (Mitsuta et al. 1986).

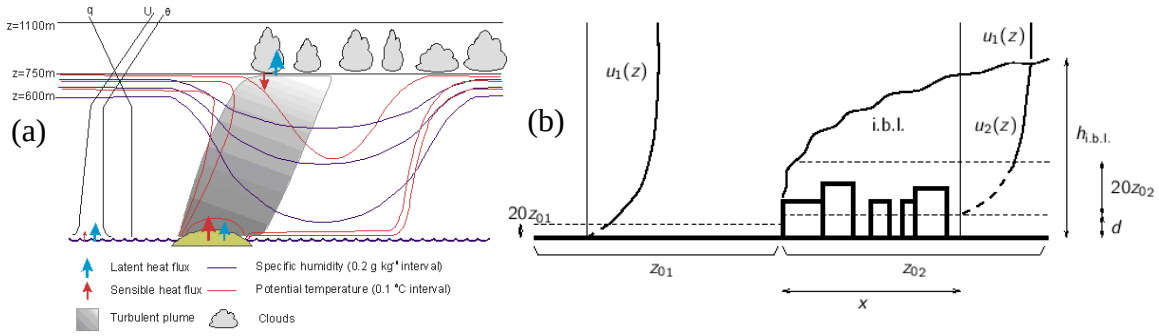

Figure 2. (a) An illustration of a TIBL produced by diurnal heating (Matthews et. al 2007). The upwind profiles of potential temperature, specific humidity, and wind speed are shon on the left side of this figure; (b) an illustration of an IBL produced by surface roughness change (van Mook 2002). Here, the IBL height is denoted at $h_{i.b.l.}$, d denotes the displacement height associated with the dense high elevation buildings.

B. ISLAND EFFECTS TO ATMOSPHERIC FLOW

Although the IBL exists with the presence of significant surface property change, it is most frequently encountered in the vicinity of an island. Matthews et al. (2007) identified three types of atmospheric circulation associated with islands of varying size and relief. There is circulation around large islands with mountains such as Hawaii's Big Island, many of the Aleutian Islands, and St. Vincent where mountains of significant height block atmospheric flow under typical conditions. A second type of island circulation is found with other large islands that lack the topographic relief of the previously mentioned islands. The third type of circulation is associated with small islands that are unable to produce significant sea and land breezes. However, the surface layer will adjust to the changes in surface forcing from roughness and heat fluxes that an island causes, which lead to downwind gradients of atmospheric parameters such as wind speed, air temperature, and humidity until a new equilibrium is reached at some distance down wind. Such changes may be significant enough to produce convective clouds. Claussen (1987) also found that the IBLs can and do, for a short distance, affect the upwind atmospheric structure.

Previous research into the interaction and impacts on the atmosphere due to the presence of a remote island has centered on Hawaii's big island's impacts on the structure

and path of tropical cyclones, wind and precipitation shadow, as well as oceanographic current wake. Other extensive research on the island effect covered the Atmospheric Radiation Measurement (ARM) on Nauru in the Western Pacific and its modification of the boundary layer, specifically the presence of downwind convective cloud streets that reach up to 120 km. There has also been extensive research and documentation of the urban heat island and its effects on boundary layers. The following summarizes the specific island effects from the above-mentioned studies to illustrate the variety of responses of the atmosphere to islands of different properties.

1. The Urban Heat Island Effect

As reported by Arnfeld (2002) the enormously complex urban heat island (UHI) has been well documented and observed for decades. Kim (1992) pointed out that the climate alterations were unperceivable prior to changes that commenced in urban growth after WWII. The most obvious properties to promote changes in the energy budget of an urban environment are the roughness, albedo, and moisture availability. Arnfeld (2002), Kim (1992), Stull (1988) and Sass (2012) identified UHI as due to albedo changes, anthropogenic heating, surface roughness changes, latent heat reduction, and atmospheric pollution such as aerosols and photochemical smog. One of the main impacts of urban environment on the atmosphere is the establishment of a roughness sublayer where individual structures lead to wakes or plumes of heat, humidity and pollutants. This effect is blended and damped with distance from the urban structures; however, the roughness sublayer can reach a depth that is several times higher than the highest structures in a particular urban environment (Arnfeld 2002). Additional turbulence from the roughness sublayer also has a significant impact in the energy fluxes between the urban surface and the surrounding atmosphere. Changnon (1981) also found that the prevalence of condensation nuclei from pollution along with a deeper mixed layer due to surface convergence and entrainment from turbulence led to precipitation events directly downwind of an UHI.

One of the significant impacts of urban heat islands is the modified radiation budget and the subsequent differential heating. Modern structural and urban codes

require the use of asphalt, concrete, and other non-porous building materials that have albedos and heat capacities that absorbs more incoming radiation and release the additional energy to the lower atmosphere through the sensible heat flux. This leads to surface layer temperature increases compared to the countryside. Figure 3 depicts the isotherms associated with an UHI during the daytime. The high temperature over the urban area is apparent in this figure. The UHI effect also experiences the diurnal cycle but is most pronounced at night when the country side cools quickly and the increased surface area and heat capacity of urban buildings leads to the radiative heating of the nocturnal surface layer. Other UHI effects include enhanced turbulence, counter-rotating vortices on opposing sides of a city, and horizontal temperature gradients leading to wind speed increases (Draxler 1986; Balling and Cerveny 1987). The increased longwave radiation due to the urban environment comes from increased warmth of the urban atmosphere, enhanced atmospheric emissivity from pollutants, and buildings heated by direct and indirect short-wave radiation. Kim (1992) found the preferential heating of urban environments to be as much as 10°C as compared to nearby wooded areas. Oke (1982), in addition to Katsoulis and Theoharatos (1985), related the UHI temperature difference to city size with small cities of 1,000 people only having a temperature differential of 2 to 3°C when compared to local countryside.

Figure 3. A depiction of the isotherms associated with an urban heat island (Image from the Arbor Day Foundation at arbourday.org).

2. Island Effects on Tropical Cyclone Track and Intensity Modification

Islands with topography may have significant upstream and downstream impacts on the boundary layer and beyond. Chambers and Li (2011) found that the unique topography of Hawaii's Big Island had significant impacts on atmospheric flow over and around the island. Under typical wind conditions the Froude number associated with the Big Island indicates that it is blocking flow from going over the island. The Froude number is often referred to as the ratio of inertial to buoyancy forces and can be expressed as

$$Fr = \frac{\pi M}{N_{bv} W_T}$$

Where M is the air parcel's mean wind speed, N_{bv} is the Brunt-Vaisala frequency and the width of the obstacle is W_T (Stull 1988). Low Froude numbers lead to the flow going around the obstacle due to blocking. As the Froude number increases with stronger winds or weaker stability the flow is able to force its way over the obstacle and this can lead to mountain lee waves, lenticular clouds, boundary layer separation, or turbulent wakes downwind. The ultimate conclusion Chambers and Li found from their idealized and real case tropical cyclone (TC) model simulations was a slowing of the track for storms approaching from the east. TC's that track to the south of the Big Island are deflected to the south. Once in the lee of the island some TC's have been shown to deviate to the north as they have entered the region where the big island wind shadow reduces the prevailing easterly trade winds. Figure 4 displays the tracks for all TCs, tropical depressions, and tropical storms from 1947 through 1997 that passed within 200 nautical miles of the Hawaiian Islands. All together the Big Island acts as a protective shield to the smaller Hawaiian Islands for storms that approach from the east but may increase the danger to the smaller islands for storms tracking from the south. This increased hazard was surmised by Chambers and Li (2011) from a case study of a more northerly track of Hurricane Dot in 1959 as it passed to the south of the Big Island that ultimately made landfall on Kauai.

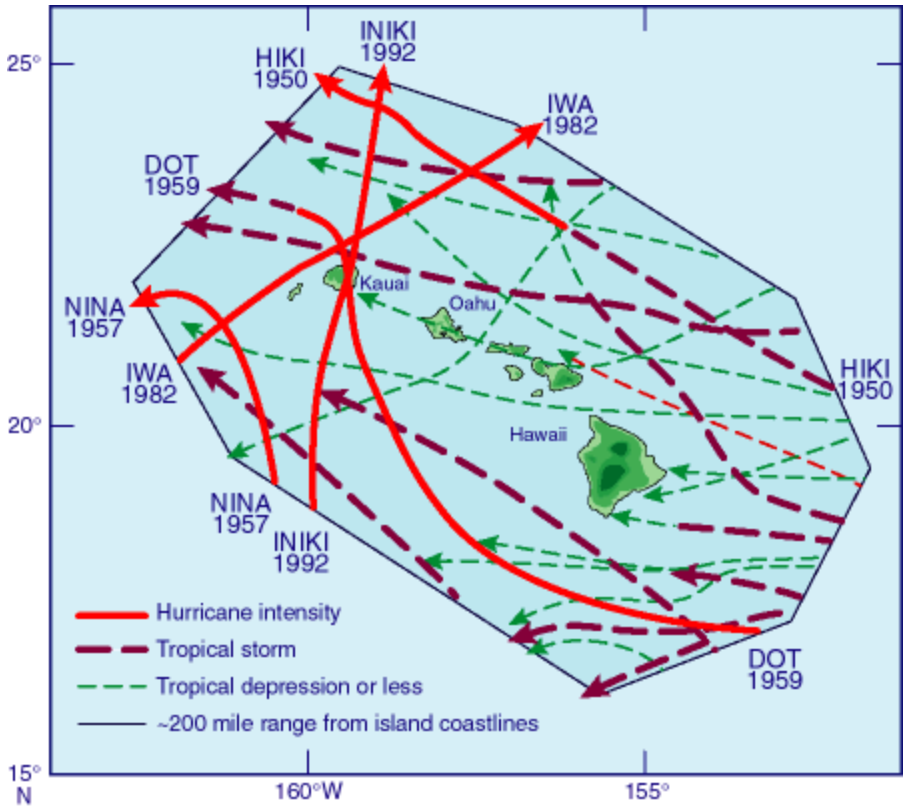

Figure 4. Tracks of all tropical disturbances passing within 200 nautical miles of the Hawaiian Islands from 1947 through 1997, from the State of Hawaii Government website at Hawaii.gov, 2012.

3. Island Effects on Boundary Layer Measurements

Islands have been frequently used as the bases for long-term monitoring of environmental parameters and the data have been frequently used to represent the marine environment nearby. During the mid-1990s the U.S. department of Energy (DOE) undertook a study of the global climate and a part of that study was the ARM. The Nauru99 field project associated with ARM was carried out between June and July of 1995 with the aim of increasing climate model parameterization of clouds and radiation by examining the island effect and relating the island-based measurements to data collected over the ocean (Matthews et al. 2007; McFarlane et al. 2004). Nauru99 field project included the NOAA research vessels *Mirai* and *Ronald H. Brown* in addition to an Australian Cessna research aircraft. There are now three ARM sites in the Tropical Western Pacific Ocean (TWP): Manus Island in Papua New Guinea, Nauru, and Darwin

in Australia. It was found that the presence of Nauru, due to the roughness and increased heat capacity of the island as compared to the ocean environment surrounding the island, led to the development of a TIBL. The roughness of the island reduced the surface layer wind speed while the buoyancy and convective mixing above the island increased the wind speed. Matthews et al. (2007) concluded that the island generated a TIBL of 600 m in depth and this modified MBL was advected 15 to 20 km downwind of the island. In addition, the convection from the island produced long plumes of cumulus clouds. Matthews et al. (2007) surmised that convective rolls supported and continued the cloud plume downwind of the island with distance in excess of 100 km. McFarlane et al. (2004) stated that the island heat plumes set up roll vortices that kept the cloud plume moving downstream and that orographic lifting was not a mechanism for cloud production. A graphic of the Nauru island effect can be found in Fig. 5. While there was a specific island-induced impact to the MBL, the Nauru99 experiment and the use of island based measurements for ARM was validated as the clouds only reduced the island based measurements of downwelling longwave radiation by 1 to 2%, which is less than 10 W m^{-1}. Long and McFarlane (2011) were able to confirm conclusions from McFarlane et al. (2004) with five years of data and quantified the impact of the island-induced clouds on Nauru measurements for climate research. They found an increase of low-cloud base height by 15-20% on Nauru, which occurred 11% of the time during daylight hours only. The aggregate effect on downwelling shortwave radiation was 2% for daylight hours and half of that for the daily average. Longwave radiation modification by the island-induced clouds was shown to be less than 2%. It was also noted that the orographic lifting of the air parcels due to Nauru's 60 m relief was not a factor in producing clouds.

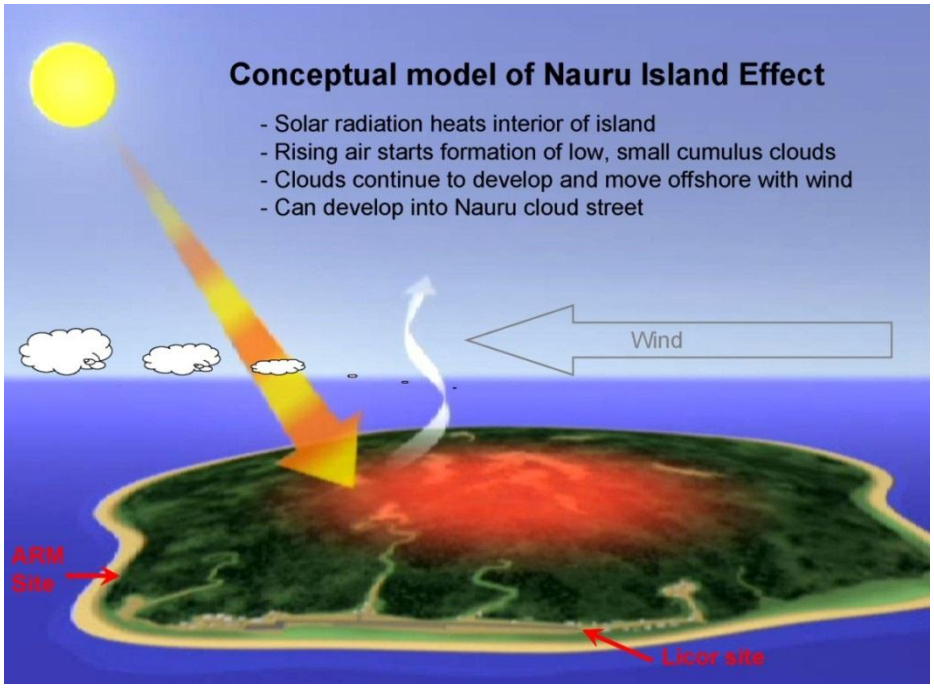

Figure 5. Conceptual picture of Nauru island effect from Long and McFarlane (2011). The two sites identified are locations of continuing in-situ meteorological measurements as part of the ARM research project.

III. DATA

A. OVERVIEW OF DYNAMO

1. DYNAMO Field Project.

The goal of the DYNAMO project is to accelerate the understanding of key processes in Madden-Julian Oscillation (MJO) and especially the initiation of the oscillation. DYNAMO was the field campaign of CINDY-2011 (Cooperative Indian Ocean Experiment on Intraseasonal Variability in Year 2011), which was an international project, running from October 2011 through March 2012, with Australia, India, and Japan participating (Zhang et al. 2011). The motivation for the U.S. field research of the DYNAMO project was driven by the current problems in prediction skill for the MJO and the lack of skill for state-of-the-art global forecast models in handling MJO. The lack of skill in global forecast models handling of MJO reduces their seasonal to interannual prediction statistics and confidence. The design of the project was to collect observations required to test hypotheses of the structure and evolution of clouds, the interaction of the clouds with larger-scale environment, and air-sea interaction. The three DYNAMO hypotheses are Hypothesis I: Deep convection can be organized into an MJO convective envelope only when the moist layer has become sufficiently deep over a region of the MJO scale; the pace at which this moistening occurs determines the duration of the pre-onset stage. Hypothesis II: Specific convective populations at different stages are essential for MJO initiation. Hypothesis III: The barrier-layer, wind- and shear-driven mixing, shallow thermocline, and mixing-layer entrainment all play essential roles in MJO initiation in the Indian Ocean by controlling the upper-ocean heat content and SST, and thereby surface flux feedback.

In-situ vertical profiles and sensing of the environment was accomplished with aircraft based measurements, dropsondes launched from the aircraft that will be discussed in depth in section B of this part, a radar network to include shipboard C- and W-band Doppler radars and an island network of radars, two ships and a network of moored sensors. The measurements were taken from a trapezoidal shaped area bounded by Diego

Garcia in the southwest, the island of Gan in the Maldives just south of the equator to the northwest, the research vessel R/V *Roger Revelle* anchored to the northeast, and the research vessel R/V *Mirai* was anchored to the southeast. The geometry of the projects design can be seen in Fig. 6.

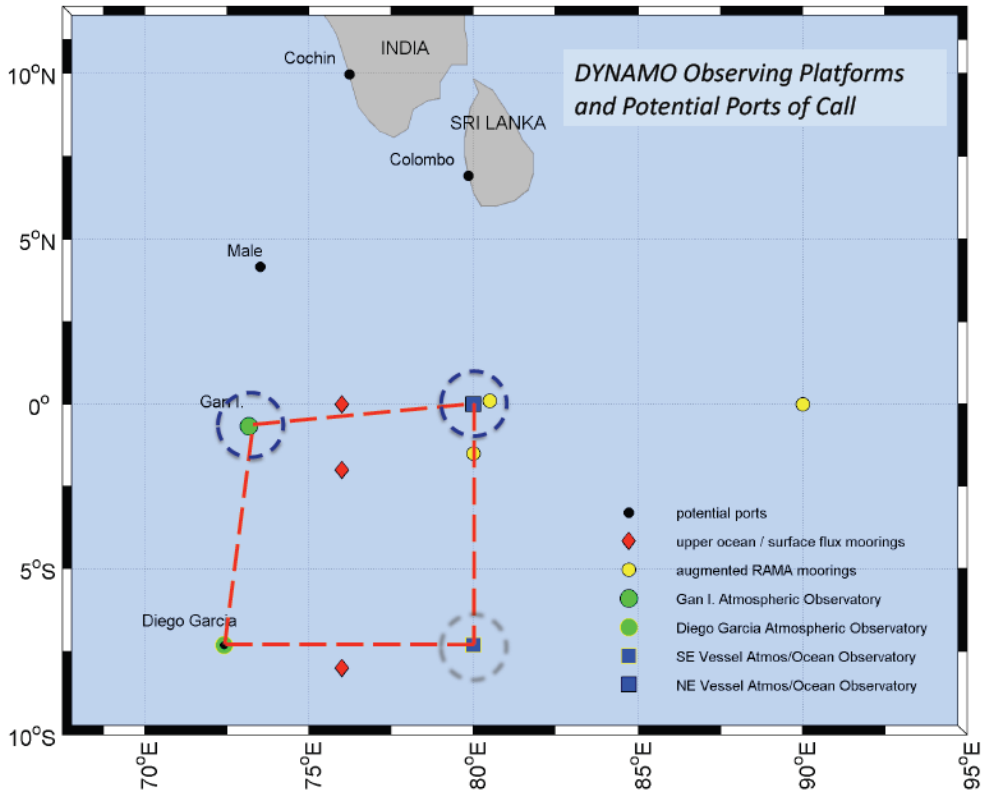

Figure 6. Depiction of the DYNAMO sounding array (Zhang et. al 2011).

Data analysis of the in-situ meteorological and oceanographic measurements from the array of sensors, platforms, and locations mentioned above will be augmented with satellite data and model reanalysis to establish model boundary conditions and constraints in order to facilitate validation and evaluation of the models. The project consists of four integrated sets of research: a field campaign, data analysis, modeling, and forecasting. The measurement plan for the DYNAMO field project was broken into three specific periods. All of the observation periods started on 01 October 2011 with the special Observation Period (SOP) running through 09 November 2011, the Intensive Observation

Period (IOP) ended on 05 January 2012, and the Extended Observation Period (EOP) was scheduled to continue through 31 March 2013.

2. Geography and Environment of Diego Garcia

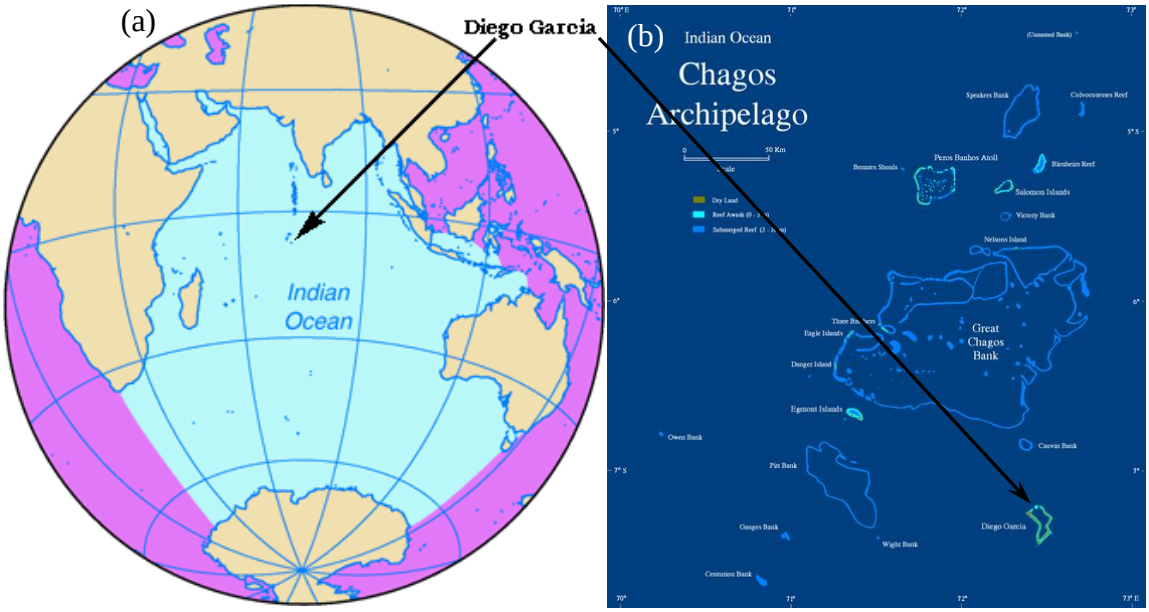

Figure 7. (a) Map of the Indian Ocean (image from U.S. Navy, http://www.nctsdg.navy.mil/). (b) A large scale map depicting the Chagos Archipelago (Image from Mohonu, en.wikipedia). Diego Garcia's location is marked in both images.

Diego Garcia is part of the British Indian Ocean Territory (BIOT) and is the largest land mass in the Chagos Archipelago in the equatorial Indian Ocean. Diego Garcia's specific location is 7°26' south and 72°23' east (-7.313S, 72.414E), which places it 1,200 miles south of the Indian subcontinent and 1,800 mile east of Africa. Fig. 7 depicts the location of Diego Garcia in the Indian Ocean and its relative size and location compared to the rest of the Chagos Archipelago. The continuous portion of the Diego Garcia foot print shaped atoll is 64 km (40 mi) long and all but surrounds a lagoon that measures 21 km (13 mi) long and 11 km (7 mi) wide at its widest point with a 6 km (4 mi) wide mouth on the northern end. The island and lagoon occupy 169.6 km^2 (65.6 mi^2) of which 124.1 km^2 (47.9 mi^2) is the surface area of the lagoon. The greatest depth within the lagoon is 25 m (80 ft.) but a significant portion of the lagoon is less than 10 m

(33 ft.) in depth. The highest point on the island is the ever shifting peak of several dunes that range in height from 4.5 m to 9 m high (15 to 30 ft.). Figure 8 shows the lagoon bathymetry and general shape and size of the island. There is a fringing coral reef surrounding the ocean side of the island that is approximately four feet below mean sea level and 91 m wide (300 ft.). There are portions of the coral reef that reach up to 198 m wide (650 ft.) and all told the reef's surface area measures 35 km^2 (14 mi^2). The ocean depth on the north and west side of Diego Garcia is limited by the Great Chagos Bank at 1000 m (3300 ft.). To the east and south the ocean depth drops off precipitously to 5,000 m (16,400 ft.) or deeper with the north-south Great Chagos trench (U.S. Navy 2005; Stoddart and Taylor 1971). Figure 9 shows the bathymetry surrounding Diego Garcia.

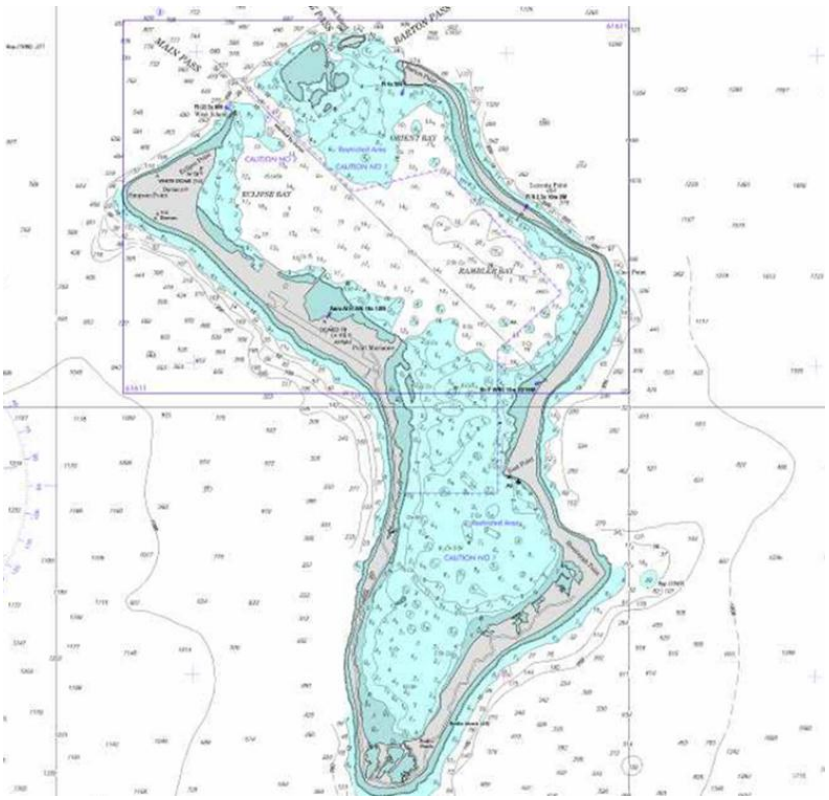

Figure 8. Nautical chart of Diego Garcia. The blue-shaded region has a depth of 10 m or less. (Image from Maryland Nautical Sales, http://mdnautical.com/).

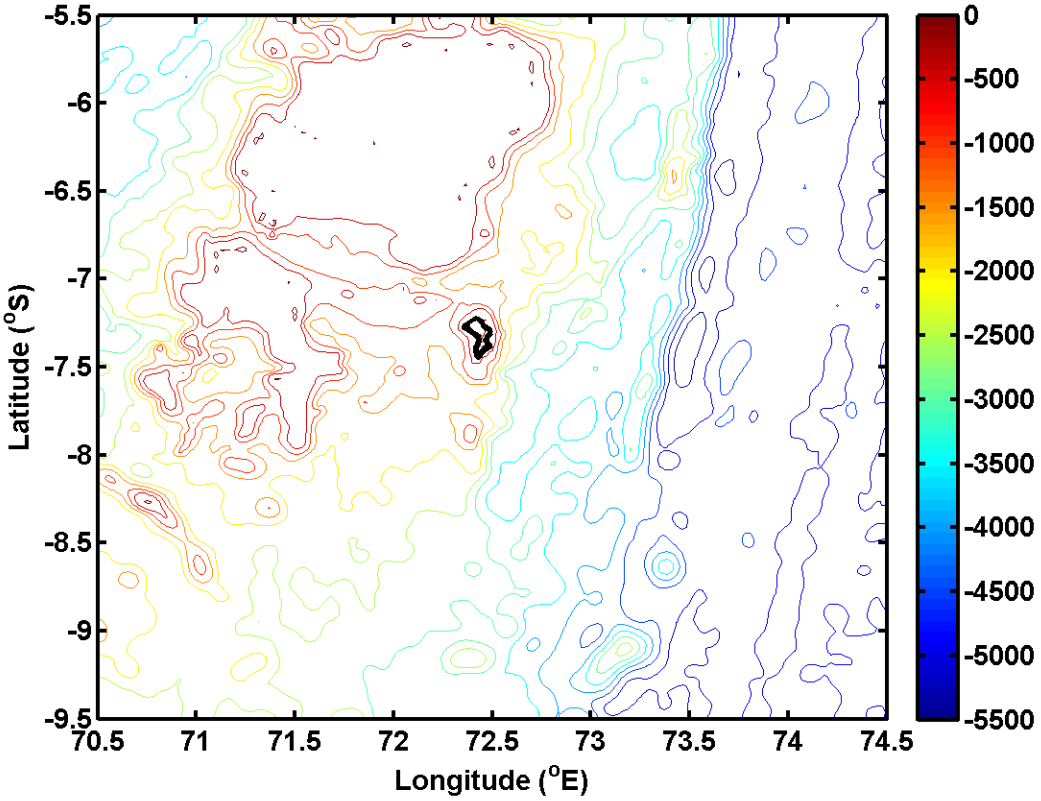

Figure 9. 1 Arc-minute resolution bathometric chart of the Indian Ocean surrounding Diego Garcia. Depth is in meters produced with data from Amante and Eakins (2009).

The climate of Diego Garcia is distinctly tropical as the island is seven degrees south of the equator. Light breezes dominate throughout the day as does sunshine, warm temperatures, and sporadic rain showers. There is a dryer season from June through September that also sees slightly cooler temperatures. The most rain falls during the December through February months. The total annual rainfall is 260 cm (102 in.) with small cumulus clouds typically scattered throughout the area and an all but complete lack of fog. The average daily temperature is fairly consistent year round at 27°C (81°F) with slightly cooler temperatures during the dryer June through September months and slightly higher temperatures in December, January, and February. The wind varies with the wet and dry seasons. The winds during the first four months of the year are predominately westerly or northwesterly at 5-10 m s^{-1} (10 to 20 knots). Following a two month transitional period with light and variable winds, the months of June through September

see slightly stronger southeasterly winds of 8-12 m s^{-1} (15-24 knots). October through December again see a transition of the wind from the southerly trades to the northwesterly and westerly. Diego Garcia is within the south equatorial current all year and as such the ocean temperatures remain between 26° and 28°C, and do not experience a wide seasonal change (U.S. Navy 2005; Forecaster's Handbook 2002; and Stoddart and Taylor 1971).

B. DROPSONDE DEPLOYMENT

Testing of Hypotheses I and II of DYNAMO requires accurate profiles of atmospheric parameters such as moisture, temperature, wind speed and direction. These vertical profiles, which capture the large-scale structure of the atmosphere through the sounding network, can be reliably measured by the use of soundings from aircraft-based dropsondes, island/ship-based upsondes, and remote sensors such as lidars or wind profilers. In order to capture the large-scale atmospheric structure DYNAMO utilized the P-3 and GPS Vaisala dropsondes in addition to GPS upsondes being launched four times a day from the four corners of the project area mentioned above during the IOP and eight times a day during the SOP. The specific upsonde used at the surface locations was the Vaisala RS92 GPS sondes with MW31 ground station processing subsystem operating on Digicora III software. In order to capture a more complete picture of the synoptic scale atmospheric structure increased soundings from other Indian Ocean locations was included as part of DYNAMO's field project. The addition sounding locations were from the Seychelles, Cocos, Darwin, and DOE's ARM site at Manus.

The dropsondes used were the RD94 GPS dropsondes that measure the temperature, pressure, relative humidity, wind speed and direction while falling from the launch altitude to the surface. Figure 10 show a picture and conceptual drawing of a dropsonde. As reported by Hock and Franklin (1999) decent rates for a dropsonde changes depending on the altitude. The maximum launch altitude is 14 km and this calculates to a 15 minute decent duration. For the DYNAMO project dropsondes were launched from either 22,000 ft or 10,000 ft with initial fall velocities of 18 m s^{-1} and 15 m s^{-1} respectively. With the square-cone parachute, the fall velocity at sea level is about 12 m s^{-1}. The Wind speed and direction is measured four times a second (or 4 Hz) using

GPS receiver and custom firmware. The pressure, temperature and humidity are each measured two times a second (or 2 Hz). Due to the fall rate and temporal resolution, typically the last pressure measurement registered and transmitted by a dropsonde is within 6 m above the surface. Dropsondes require specialized launchers for pressurized and non-pressurized aircraft and require equipment to receive and process the data onboard the aircraft.

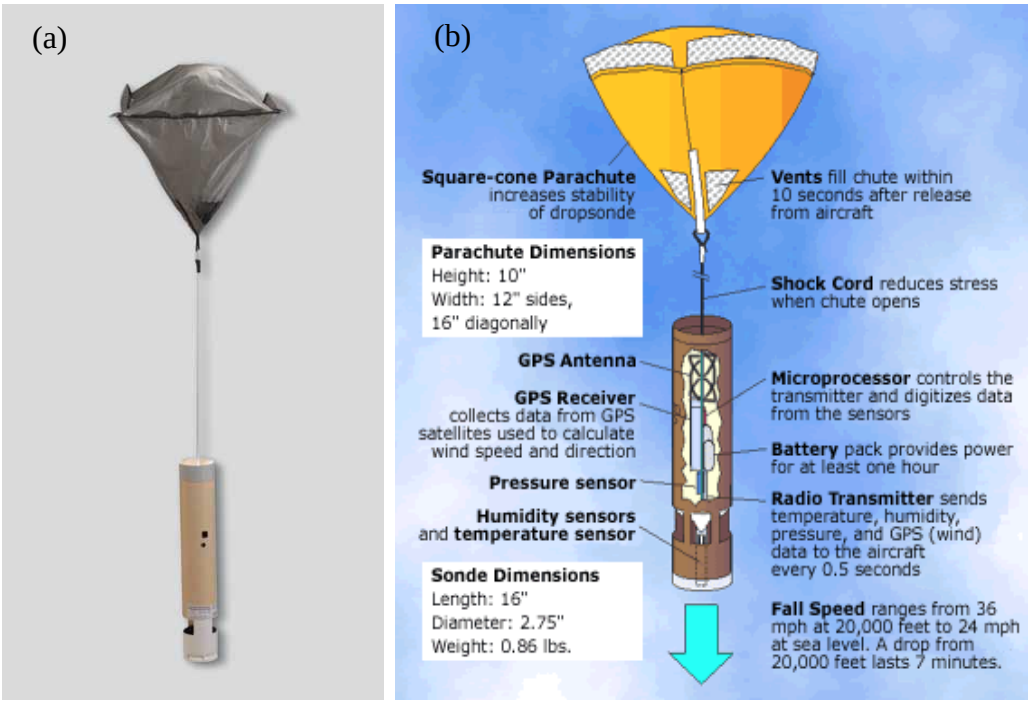

Figure 10. (a) A picture of the Vaisala RD94 GPS dropsonde. (b) An exploded view of a dropwindsonde (Images from Vaisala, http://www.vaisala.com/ and NASA, http://earthobservatory.nasa.gov/ respectively).

The flights of the P-3 were conducted during the IOP and consisted of 12 flights in all for 105 flight hours. Ten of the flights were for research specific goals with the initial flight for testing and the last flight for calibration. The test and calibration flights were flown in accordance with the two primary goals of DYNAMO, convective and boundary layer process, and as such the flight can be divided into six boundary layer

centric flights and six convective centric flights. Figures 11 and 12 illustrate the flight paths of the respective investigation goals.

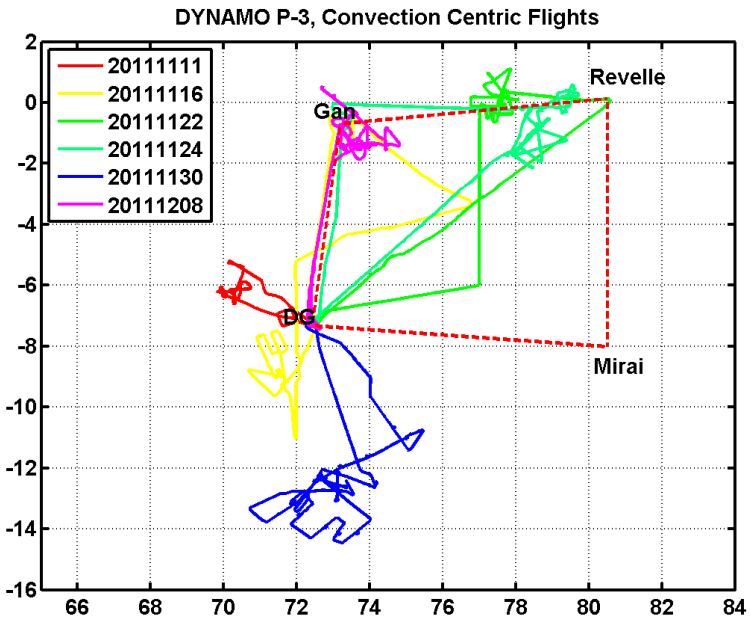

Figure 11. Flight tracks of the six convection centric flights. The flight dates are given in the legend in yyyymmdd format.

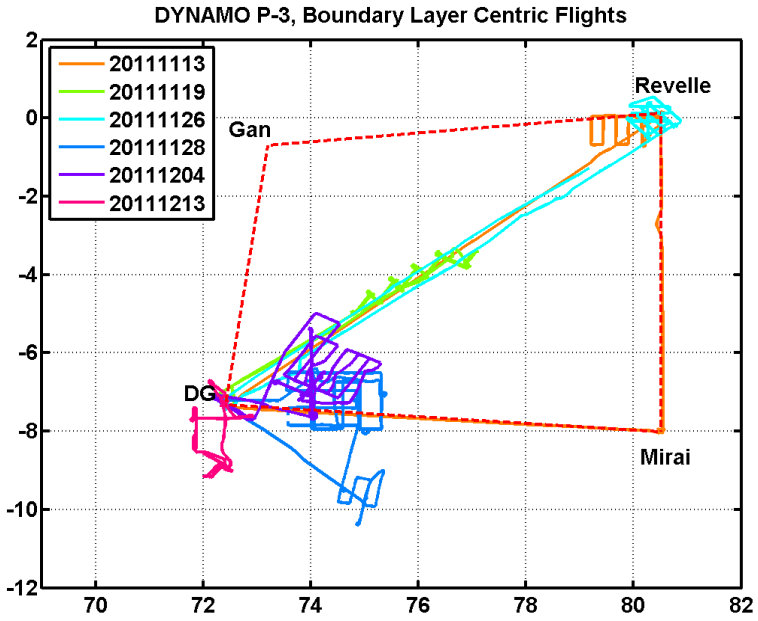

Figure 12. Flight tracks of the six boundary layer centric flights. The flight dates are given in the legend in yyyymmdd format.

Table 1. Summary of all DYNAMO P-3 flights.

Flight date (yyyymmdd)	Objective	Description	Take off - Landing time (UTC)	Modules (minutes)	Drop-Sonde	BT/CTD
20111111	Instrument and operation test	test of flight level sampling, dropsonde, BT/CTD, and radar NW of DG; convection sampling NW of DG	07:03 - 10:34	1 RCE (21)	5	4/2
20111113	Large-scale SST/Moisture gradient and air-sea interaction close to Revelle	large-scale sampling DG to Mirai (D/B), Mirai to Revelle (D), and Revelle to DG (D/B); BL sampling west of Revelle	03:12 - 12:34	1 FVS (53),1 FFM (71), 2 LSS (229) at 10000', 1 LSS (106) at 25000', OH (117)	49	46/4
20111116	Large-scale Moisture variability and convection	South of DG for convection, large scale survey west of DG (D/B), towards center of SDA (D), center of SDA to Gan (D), and Gan to DG (D), Dropsondes near SPol	04:06 - 13:02	1 FFM (56), 1 RCE (43), 3 MP (14), 1 LSS (97) at 10000', 3 LSS at 25000' (114), 1 FD (16), 1 Gan dropsonde (24), OH (182)	55	24/16
20111119	BL in suppressed phase with small cumulus, large-scale variability	BL towards center of SDA, large-scale variability from center of SDA to DG (D)	03:43 - 12:29	5 FVS (371), 1 LSS at 25000' (53), 2-level turb legs along the track (116)	16	9/17
20111122	Multiple convective systems in onset phase of MJO and large scale variability	Convective sampling at the equator midway between Gan and Revelle, large-scale between N-S median of SDA (D), diagonal of SDA, and near DG (D)	02:06 - 12:08	1 RCE (44), 2 FLX (101), 3 MP (16), 1 LSS at 10000' (90), 2 LSS at 25000' (129), 1 FD (14), 1 RB (34), OH (191)	51	20/11
20111124	Multiple convective systems in onset phase of MJO	Convection southwest of Revelle, large scale variability along the Revelle, Gan, and DG triangle (D), dropsondes near SPol	01:28 - 11:17	2 RCE (102), 1 FLX (39), 1 MP (11), 3 LSS 25000' (186), 1 FD (22), 1 Gan drop (12), OH (234)	57	7/2
20111126	Large-scale SST/Moisture gradient and air-sea interaction close to Revelle	BL over Revelle, large-scale transits diagonal of SDA in the morning and afternoon (D/B/C)	03:15 - 12:53	1 FVS (65), 1 FFM (68), 2 LSS at 10000' (248), 2 FD (35), 1 RB (32), 1 SI (40), OH (106)	33	37/21

20111128	Wind and thermodynamics variability and air-sea interaction in variable cloud conditions during active phase	BL sampling in moderate westerly wind condition E and SE of DG	02:07 - 11:22	1 FVS (48), 1 FFM (102), 1 DAS (88), 1 DCE (55), 1 SI (96), OH (181)	35	28/15
20111130	Spatial variability in precipitating convective systems	convection S of DG near 14^{O}S	01:36 - 11:33	1 DCS (93), 1 RCE (44), 1 FLX (51), 1 MP (10), 1 DCE (218), 1 SI (26), OH (170)	58	18/4
20111204	Wind and thermodynamics variability and air-sea interaction in variable cloud and moderate wind conditions, DG island effect	BL sampling NE of DG	02:02 - 12:07	2 FVS (145), 1 FFM (103), 1 SI (103), 1 DAS (93), LSS (173)	43	51/4
20111208	To observe 3D structure of convective systems in coordination with Falcon and Spol	Convection S of Gan, dropsondes at SPol, large-scale survey between Gan and DG (D/B partially)	04:27 - 12:11	5 RCE (164), 2 LSS (124), 1 FD (24), 1 Gan drop (11), OH (157)	54	17/0
20111213	Instrument calibration and intercomparison	Near DG	03:09 - 07:37		12	26/10

During the 12 DYNAMO P-3 flights there was a total of 468 dropsondes launched with only two of the dropsondes that failed to process during the data analysis of this thesis; this yields a failure rate of less than one-half of 1%. Figure 13 depicts all of the location of the 468 dropsondes that were launched from the DYNAMO P-3. Table 1 lists the date, objective, flight times, and dropsondes launched for each of the 12 flights conducted during the IOP of the DYNAMO field project. Of these 468 dropsondes only 47 were launched within 100 km of Diego Garcia and are of interest regarding the effect the island has on the MBL; Fig. 14 illustrates the locations of these drops.

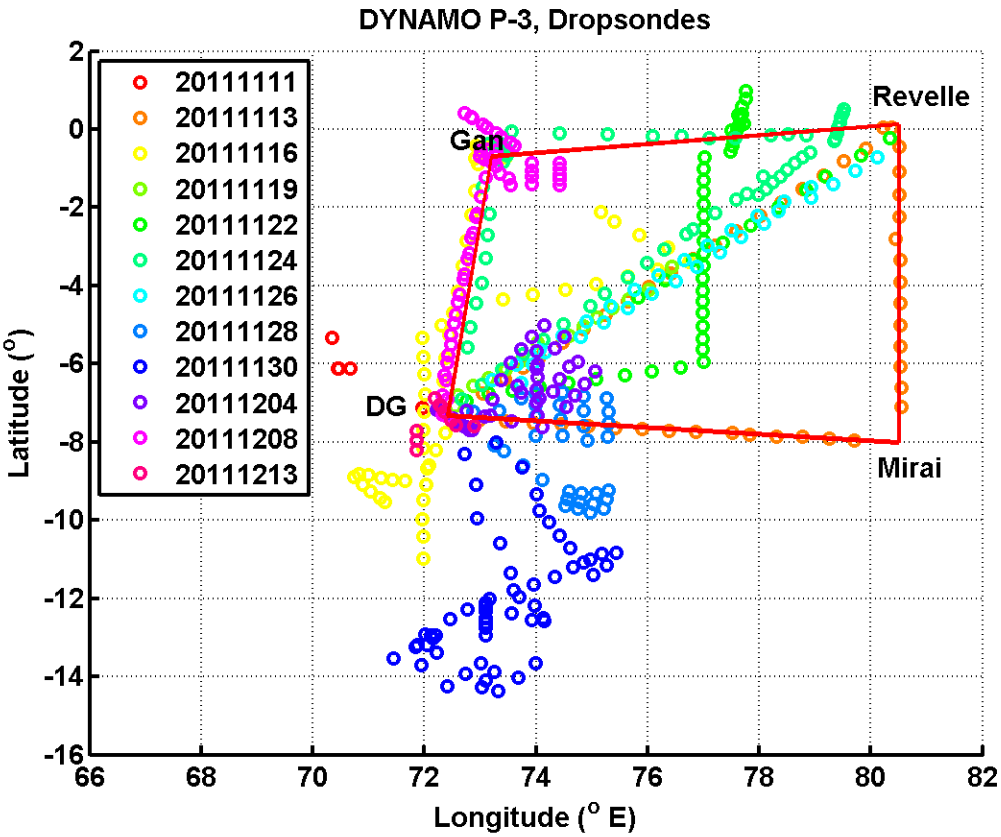

Figure 13. Locations for all 468 dropsondes from 12 DYNAMO flights. The flight dates are given in the legend in yyyymmdd format.

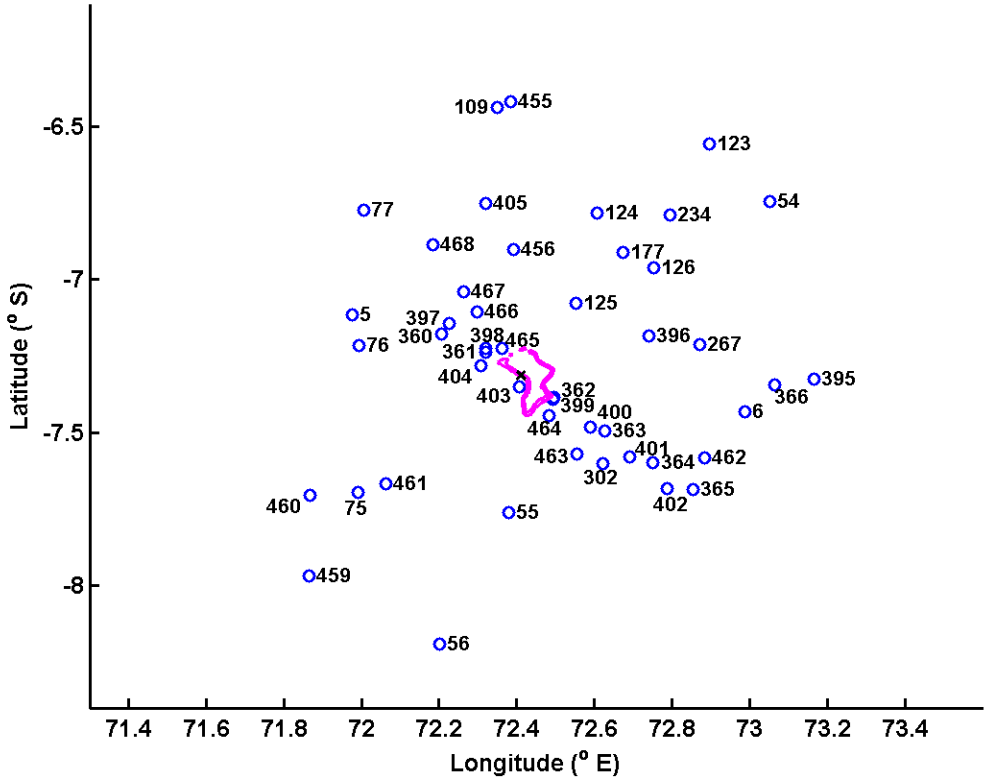

Figure 14. The 47 dropsonde locations within 100 km of Diego Garcia. The numbering is sequential starting with the first dropsonde on research flight #1 and going through the 468th from the last flight of DYNAMO. The black X on the western side of the island, just north of dropsonde #403, is the location of the end of the runway which was used for distance measurements. It is also within 200 m of the tent city from where the rawinsondes were launched.

C. DROPSONDE DATA QUALITY

Hock and Franklin (1999) reported on the accuracy and reliability of dropwindsonde's pressure, temperature, and humidity (PTH) measurements. The dropsondes use a more rugged temperature sensor, the RS-80, which has reduced sampling frequency leading to a lag in temperature measurements. This lag, approximately 1°C above 500 mb, is more pronounced at high altitudes where the dropsonde falls at a faster rate. This error is correctable to within 0.2°C by using a conversion formula in post processing. The pressure sensor has a small bias due to the flow velocity passing the static port of the pressure sensor. This bias is approximately 1-

2 mb at the surface and post processing can correct for this error by applying a systematic 0.4 mb correction. This brings the pressure accuracy up to 0.5 mb with a resolution of 0.1 mb. It takes approximately 0.5 s for the dropsonde to accomplish the PTH measurements and with a fall rate of 12 m s^{-1} at the surface the final observed measurement that is transmitted before splashdown will be between 4-10 m height. The use of a GPS receiver with the dropsondes has provided wind accuracies of 0.5-2 m s^{-1} with vertical resolution of approximately 5 m. The precision of the wind measurements approaches 0.2 m s^{-1} which is a considerable improvement over previous, non-GPS equipped dropsondes. The success rate reported by Hock and Franklin (1999) for the wind sensors was 95%.

All commercial dropsondes are equipped with two humidity sensors to facilitate quality control and accuracy of the humidity measurements. Wang (2005) reported the under-utilization of humidity data in Hurricane forecasting due to a dry bias on the order of 5 to 20% reported in previous studies. Some of the dry bias can be attributed to the age of the dropsondes or the manufacturer of the dropsondes. One manufacture, Flacon, had dropsondes that consistently showed an 8% dry bias during an extensive field study in 2002. There have also been issues with contamination bias due to packaging material, bulk head, and the outer tube. When a dropsonde is launched it can be colder or warmer than the ambient atmosphere and must reach equilibrium with the atmosphere and start recording accurate changes in the temperature and humidity. Other error sources include the known humidity time lag error associated with sensor wetting or icing. The sensor wetting and icing is expected when a dropsonde exits a cloud and the moisture has built up on the sensor and must evaporate leading to erroneous readings for a short distance. Ultimately, Wang (2005) found that there were no systematic dry biases found in dropsonde humidity data but that time lag errors do exist when a dropsonde enters or exits a cloud. Hock and Franklin (1999) reported PTH success rate of 98%

THIS PAGE INTENTIONALLY LEFT BLANK

IV. ANALYSES AND RESULTS

A. SOUNDINGS USED TO QUANTIFY ISLAND EFFECTS

The atmospheric profiles of meteorological parameters were divided into categories regarding their location and low-level, defined for this thesis as the lowest 500 m, wind direction relative to Diego Garcia. The three options relative to position and wind direction were upwind, downwind, or offset from the island if the wind direction was skew to the location of the profile and the island. The profiles that were offset from the island regarding wind direction were taken to be representative of the marine environment. A figure depicting each of the dropsondes mean location and the mean wind speed and direction can be found in Fig. 15.

The low-level structures of the atmosphere as characterized by the vertical profiles obtained during the DYNAMO field project are in general consistent with maritime tropical environment. Figure 16 shows a typical sounding depicting the MBL and its top. There was an abundance of moisture and temperature was very high though the day and night. The surface air temperature ranged from 298° to 303°K (~25°C to 30°C) and was consistent within that range throughout the day and the DYNAMO field project region. The depth of the MBL can be clearly seen on potential temperature profiles that ranged from 200 to 800 m. With a few exceptions, the relative humidity was consistently at or above 80% for each vertical profile. The wind profiles of the DYNAMO domain showed a great deal of variability of the wind speed and direction throughout the air column that was captured by the dropsondes. Most of the wind speed profiles did have a logarithmic reduction in the surface layer due to frictional interaction with the surface. There were also ample examples showing the presence of low-level jets close to the surface and/or near the MBL top.

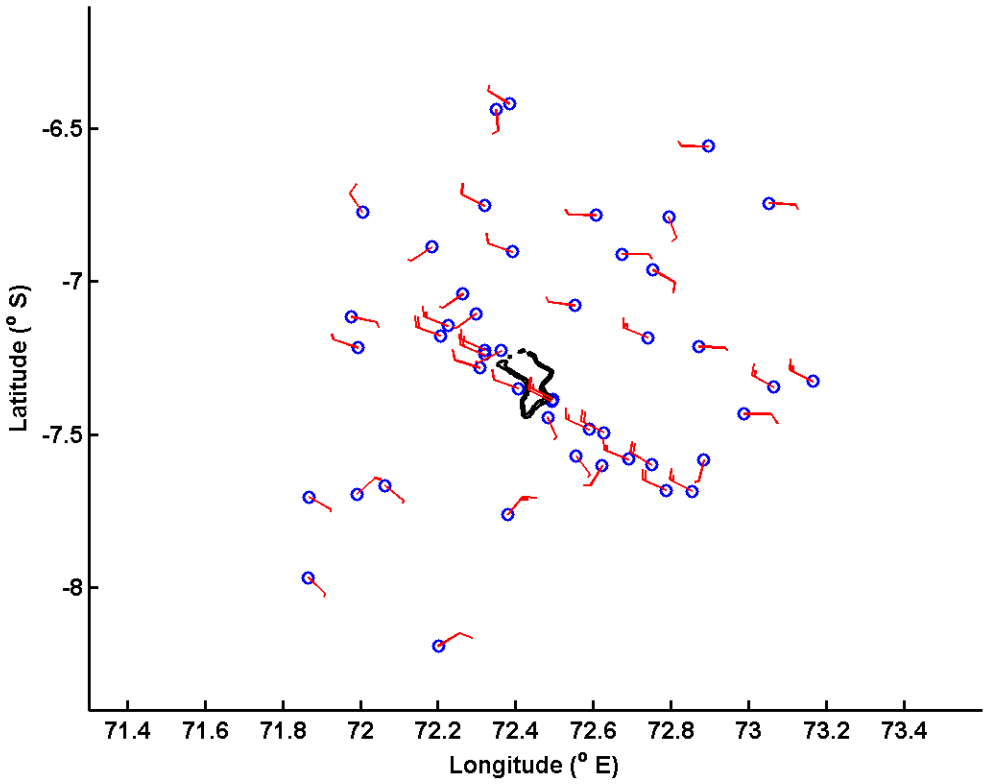

Figure 15. DYNAMO dropsondes within 100 km of Diego Garcia with wind barbs depicting the mean wind speed and direction in the lowest 500 m of the atmosphere.

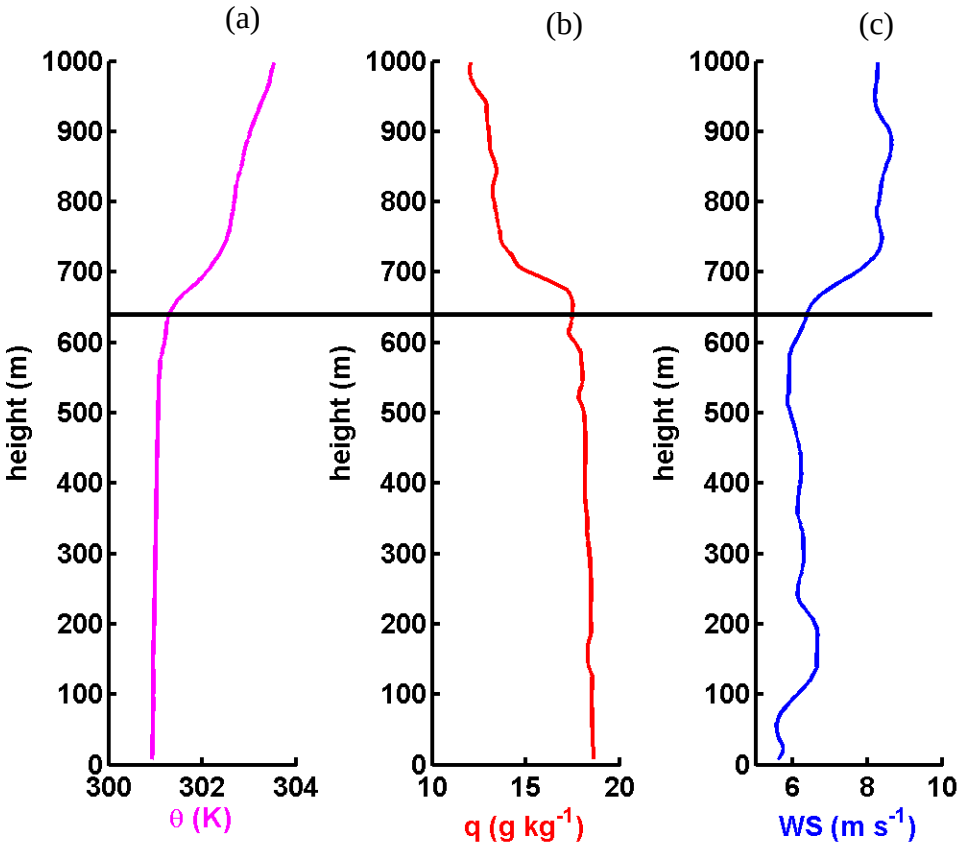

Figure 16. Typical vertical variations of (a) potential temperature; (b) water vapor specific humidity; and (c) wind speed from DYNAMO dropsonde measurements. This dropsonde measurement was made on 08 December. The horizontal black line marks the top of the MBL.

1. Moisture

One of the distinct features in the DYNAMO sounding profiles was a significant increase in specific humidity in the lowest 25 to 150 m of the atmosphere. This increase in moisture was not confined to the area around islands but was found throughout the DYNAMO field project area. This low-level moist layer will be referred to as the 'moisture toe'. An example of this moisture toe can be seen in Fig. 17 from dropsonde #5, where the specific humidity (q) increases from a 300 meter well-mixed column of 18.1 g kg^{-1} of water vapor to 18.9 g kg^{-1} in the lowest 40 m. Of the 47 dropsondes of interest to this thesis there were eight profiles that did not display a moisture toe or any moisture increase in the lowest level of the atmosphere. One of these was an afternoon

profile just downwind of the island where extensive turbulence mixing happened due to surface buoyancy from the diurnal heating of the island and the increased surface roughness. Overall the increased moisture in the lowest level of the atmosphere averaged 0.54 g kg^{-1} with an average depth of 107 m for the enhanced moisture layer. The maximum moisture increase was 1.4 g kg^{-1} that reached a depth of just over 200 m. In examining the moisture profiles from dropsonde deployment designed to study the island effects, it was clear that some of these moisture layers were associated with the presence of the island. However, with the limited number of samples, it was difficult to relate the moisture features from the rest of the soundings to a particular location or a specific atmospheric/oceanic phenomenon. It was also difficult to quantify the enhanced moisture layer characteristics, such as its depth and magnitude of moisture enhancement, due to the small difference in specific humidity compared to the moisture aloft. In the following discussion, we will focus only on the measurements from 04 December, 2011, where the soundings were made at the same time with spatial coherence.

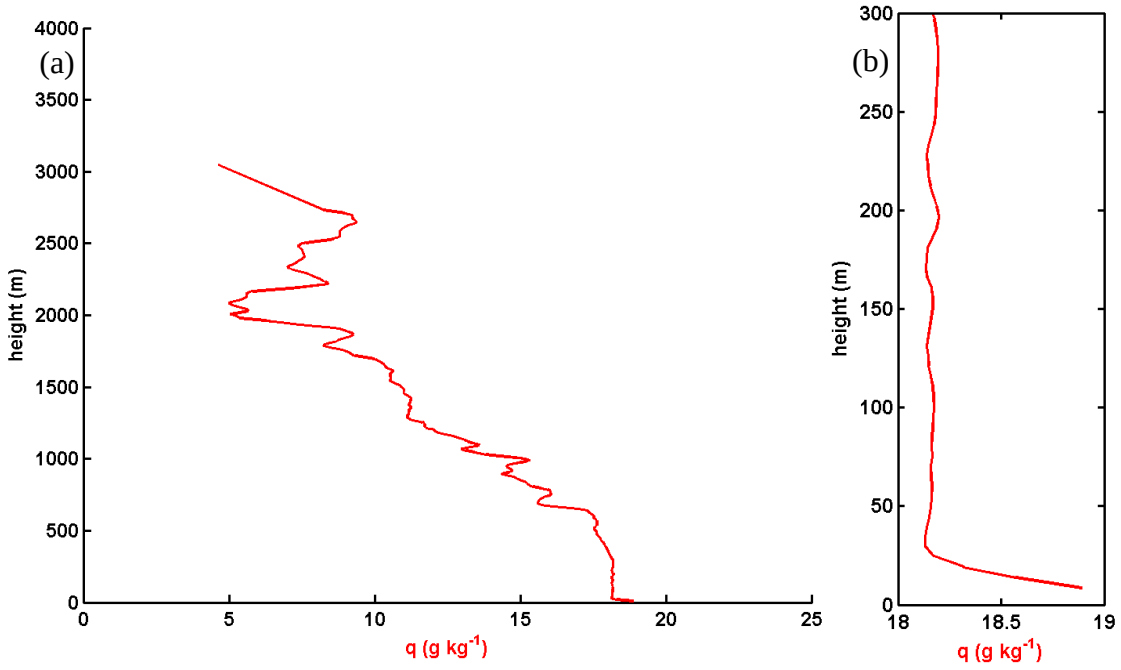

Figure 17. Vertical profile of specific humidity for Dropsonde #005, launched 11 November. (a) The full sounding from drop altitude of 3,000 m; (b) the profile of the lowest 300 m highlighting the moisture toe.

2. Wind

The wind speed profiles showed significant variability, but can be categorized into three specific categories. Fig. 18 shows examples of profiles in each category: a layer of reduced wind speed between the surface and some altitude (Fig. 18a), low-level elevated jets (Fig. 18b), and a surface-based layer of wind speed enhancement. There are some soundings (15%) where there was no discernible wind speed layer. These four types of wind layering will be referred to as a reduced layer, low-level jet, enhanced layer, and indeterminate layer, respectively. In Fig. 18a, a layer of lower wind speed can be seen in the lower 100 m compared to the wind speed above. Figure 18b show a prominent wind maximum at about 100 m above the surface with significant shear below; and an apparent wind speed increase in the lowest 40 m is seen in Fig. 18c.

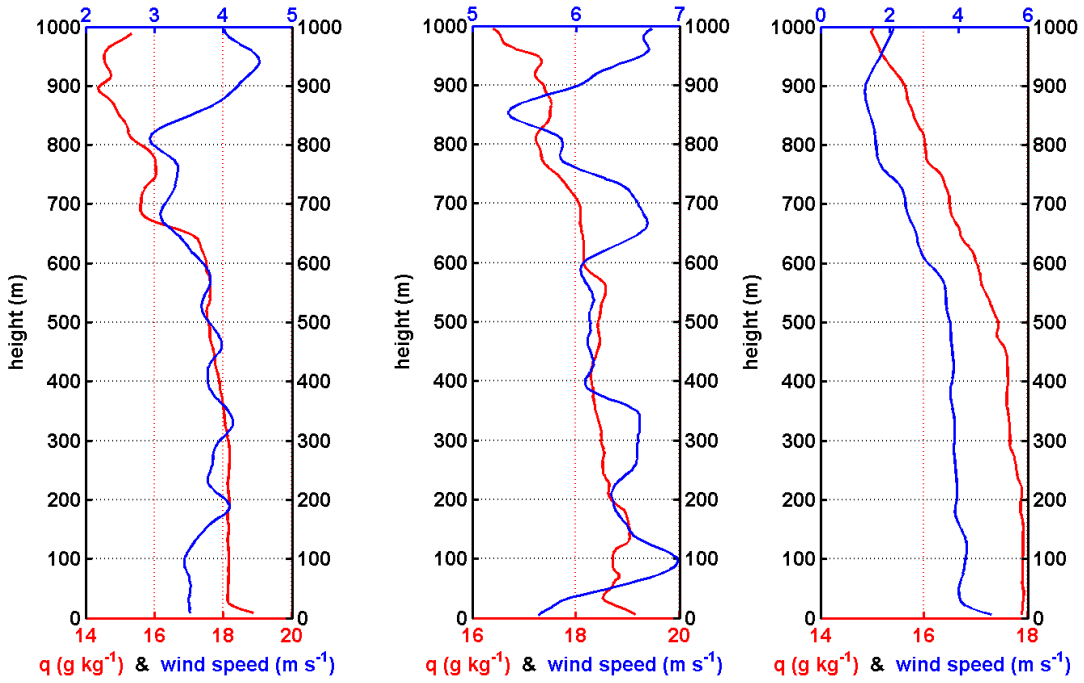

Figure 18. Three vertical profiles of wind speed depicting specific categories of wind layers. The horizontal axis across the top and the blue color corresponds to wind speed in m s^{-1} and the horizontal axis across the bottom and red color corresponds to specific humidity in g kg^{-1}. (a) An example of a wind reduction layer; (b) an example of a low-level jet; and (c) an example of an enhanced wind speed layer.

Based on Monin-Obukhov similarity theory of the surface layer (Monin and Obukhov 1954), it was expected that the wind speed profiles decreases towards the surface (log wind profiles in neutral conditions), which explains that over 50% of the wind profiles show low-level wind reduction (25 out of the 47 profiles). The profiles with a low-level jet were almost exclusively associated with offset locations: 6 out of the eight such profiles were offset and the other two were upwind. The surface-based wind speed enhancement layer was also a dominate feature of offset profiles with only one of the seven enhanced layer profiles not being offset. The occurrence of the four types of wind speed profiles are summarized according to their locations relative to Diego Garcia and wind direction (Fig. 19), where the upwind, downwind, and marine categories were based on mean wind direction in the lowest 500 m.

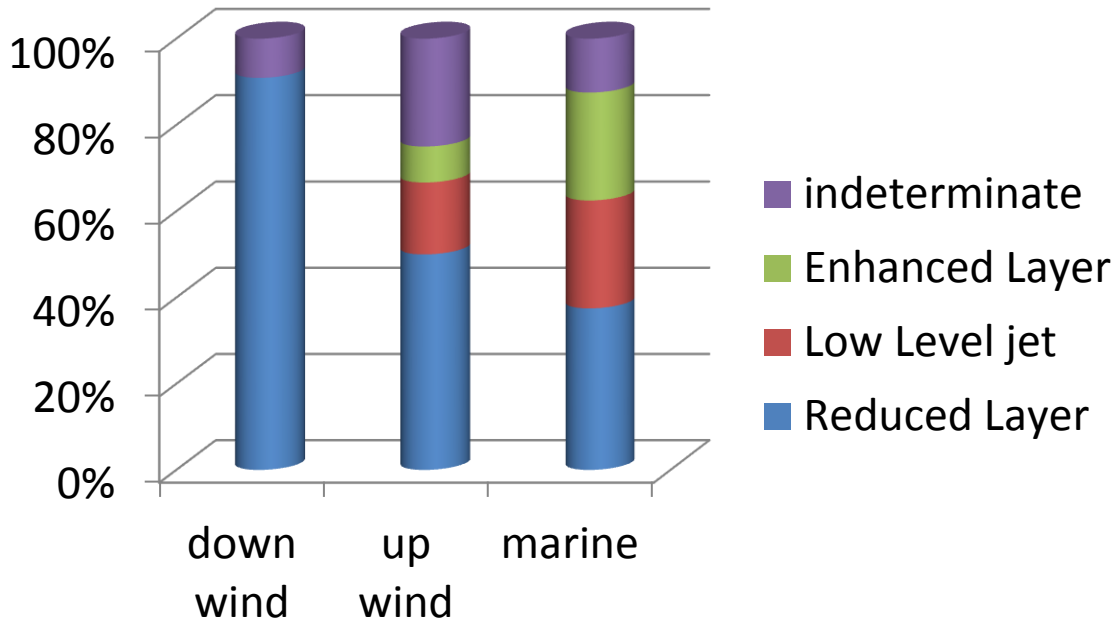

Figure 19. Statistics of the four types of low-level wind profiles observed near Diego Garcia.

Figure 19 reveals the association of the near surface wind reduction with relative location to Diego Garcia. In each of the categories the reduced layer is the dominate feature as expected. However, it can be clearly seen in the downwind category that all but 1 of the 11 profiles had a wind reduction layer. The effect of the small island on

downstream wind profiles is thus apparent. In the upwind category there was more variability but half of the profiles exhibited a reduced layer with two instances of a low-level jet, one enhanced layer, and three indeterminate profiles. The profiles representative of the marine environment saw considerable variability with a reduced layer dominating but almost equal cases with a low-level jet or and enhanced layer.

B. DIURNAL VARIATION OF SEA SURFACE TEMPERATURE IN THE LAGOON

The wind effects on the MBL because of Diego Garcia were expected and have been demonstrated in numerous previous studies on island effects. What is unique to Diego Garcia is the increase in moisture at the lowest levels, which is related to the diurnal variability of the water temperature in the lagoon to be discussed in this section. The lagoon is very shallow with a maximum depth of 25 m and approximately half of the lagoon depth is less than 10 m. The lagoon's surface area as discussed previously is 124 km^2 and it is 90% enclosed by the 64 km (40 mi) continuous atoll. This essentially makes Diego Garcia a water island. During the day, the lagoon is able to heat up faster and retain this heat due to the minimal communication with the open ocean. One of the DYNAMO measurement modules, used for the calibration of the P-3's Reigal scanning surface wave lidar, allowed for detailed SST measurements of the lagoon and neighboring open ocean. An example is shown in Fig. 20. In the morning hours the lagoon was found to be 0.75°C warmer than the ocean to the west and south (Fig. 20a). The SST in the afternoon was found to be 1.5°C warmer (Fig. 20b). The landing legs of the flights also afforded an opportunity to use the remotely sensed SST from the aircraft to compare SST from the afternoon open ocean east of the island to the lagoon's SST. There was more variability with these measurements but the minimum increase of the lagoon's SST in the afternoon was 1.5°C with several cases of over 2°C. Figure 21 displays the SST variations during the landing legs of several research flights. It is evident from this figure that the lagoon temperature was higher than the ocean surface to the east side. The higher SST in the lagoon should contribute to the enhanced surface fluxes of sensible and latent heat and thus moisture and heat plumes, all of which contributes to enhanced development of a TIBL.

A few heat plumes over Diego Garcia were sampled by the P-3 during landing descents. For each of the SST and potential temperature heat plume measurements care was taken to ensure that the data was reliable. Only SST readings on straight flight with an altitude less than 500 m were used to avoid moisture contamination of the remotely sensed SST. The landing profiles were checked to verify that there was no data used during turns or from an altitude greater than 500 m and that the temperature spikes were not correlated to the aircrafts speed or altitude/attitude angles. Examples of the profiles from takeoff and landing are shown in Fig. 22. Due to the very specific and required glide path of the P-3's landing profile, distance and height during landing were linearly correlated. As such, one can use the descent sounding to identify the nominal horizontal size of the island plumes. Figure 22a shows temperature spikes on the order of 1 to 1.5°C; these plumes have a horizontal span of appropriately 1-2 km. In contrast, the potential temperature profiles during the morning takeoff do not have significant temperature spikes; nor do the profiles away from the island. These findings suggest the effect of island-related heating and convective plumes later in the day. The same sounding in Fig. 22a is regenerated in Fig. 22b to illustrate the horizontal scale of the slant-path sounding and that the temperature spikes are not associated with the airspeed of the aircraft.

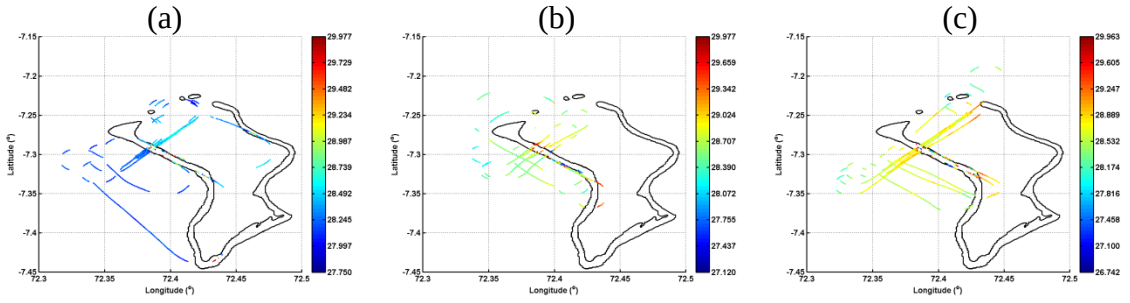

Figure 20. SST measurements during the Reigal scanning surface wave lidar (RBS) calibration runs. (a) SST from the morning RBS run with RF07; (b) and (c) SST from the afternoon RBS runs with RF05 and RF12, respectively.

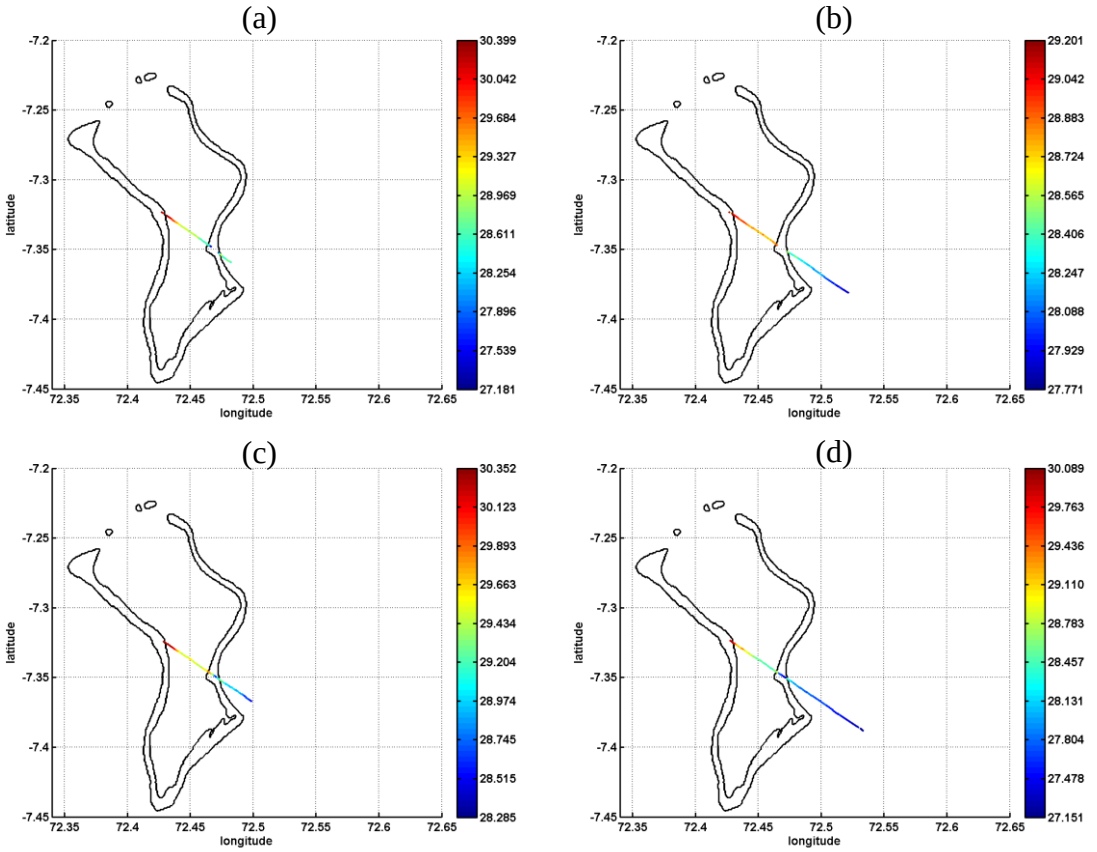

Figure 21. SST measurements during landings of research flight (counterclockwise starting from the top left) 02, 03, 06, and 10.

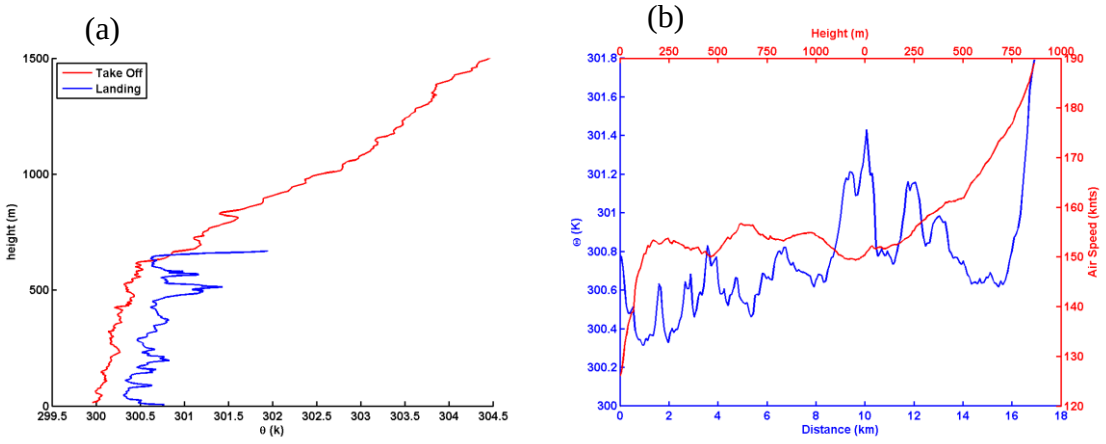

Figure 22. (a) A comparison of potential temperature profiles in the morning ascent and afternoon descent of RF08, depicting the heat plumes from Diego Garcia in the afternoon; (b) the potential temperature variation (blue) from the same afternoon sounding as in (a) except plotted again horizontal distance (top axis). The

corresponding airspeed (red) of the P-3 is also shown in (b).

C. THE ISLAND EFFECTS FROM CASE ANALYSES

Part of the mission objectives for DYNAMO RF10 on 04 December, 2011 was to capture the effect Diego Garcia has on the MBL and assess its impact on using the island-based measurements to represent the open ocean environment. On this day the synoptic conditions were dominated by mostly clear skies with a few, isolated, areas of convection that were extensively sampled by the P-3. The wind was persistently from the NW at 11.7 m s^{-1} with a maximum gust of 16.9 m s^{-1}. Sea level pressure was 1007.0 hPa and the high and low temperature for 04 December 2011 was 31.4°C and 26.7°C respectively. Far to the southwest of Diego Garcia is a weak tropical cyclone. The MJO during this research flight was active with enhanced convective activity centered across the Maritime continent. The MJO is expected to suppress rainfall over Africa and the Indian Ocean for the next one to two weeks.

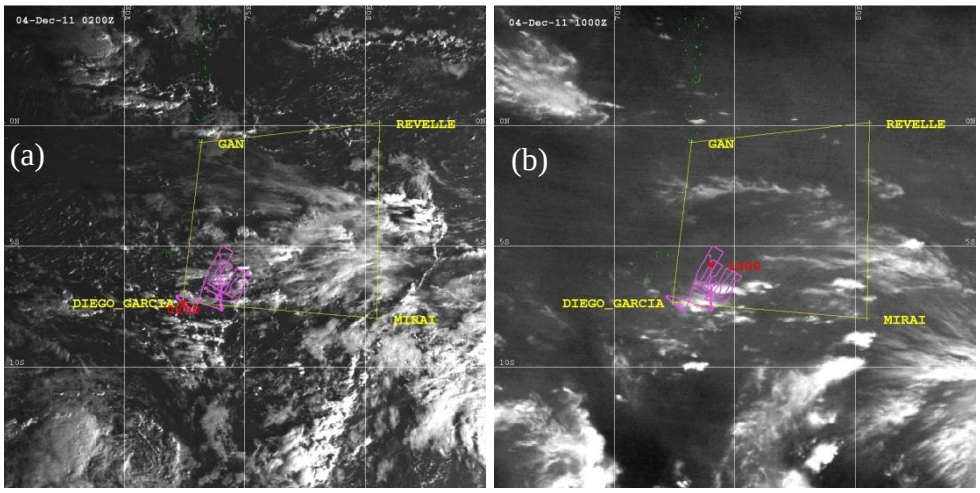

Figure 23. (a) Visual satellite cloud images at the beginning and (b) an IR satellite image near the end of the RF10 on 04 December 2011. These images indicate the evolution of cloud conditions during the flight. The flight track (magenta), DYNAMO domain (yellow), the location of the P-3 (red dot), and UTC+6 local time (red text) are shown. The GMT (z) time of the satellite image is in the upper left corner.

There were two passes over the island, one in the morning and one in the afternoon. The flight passes over the island were flown directly along or against the

prevailing low-level wind speed direction in order to capture the upwind and downwind variability and examine the modification of the MBL by the presence of Diego Garcia. There was an attempt to fly a single pass over Diego Garcia on RF12 (13 December, 2011), but the direction of the wind changed by over 90 degrees from the upwind to the downwind profile. This rendered comparison of the upwind and downwind profiles unsound for determining and examining the island effect.

Figures 24 and 25 depict the wind speed and specific humidity profiles from the morning and afternoon passes over Diego Garcia from RF10. The wind speed reduction and moisture enhancement in the vicinity of Diego Garcia in the afternoon profiles are clearly visible. Although the magnitude of wind speed reduction by Diego Garcia does not change considerably from the morning to afternoon profiles, the horizontal and vertical extent of the wind speed reduction does. In the afternoon the wind speed reduction can be seen between approximately 20 km upwind and 50 km down wind, and the depth of the effect increased from 200 m to 600 m. The presence of Diego Garcia, especially the lagoon, also increased the low-level water vapor between approximately 15 km upwind and 25 km down wind, and up to a depth of 400 m.

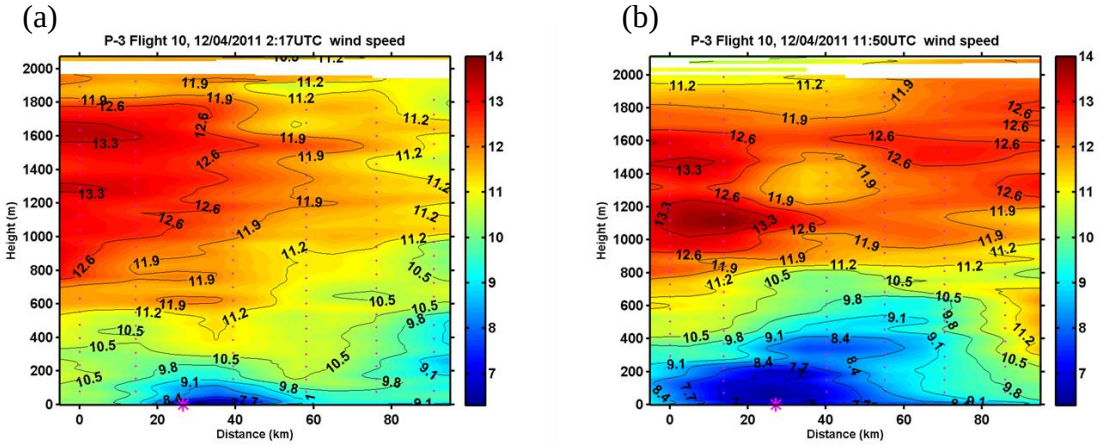

Figure 24. Contour plot of wind speed from dropsondes profiles upwind and downwind of Diego Garcia for the (a) morning and (b) afternoon of 04 December, 2011. The pink dotted lines denote the average location of each dropsonde.

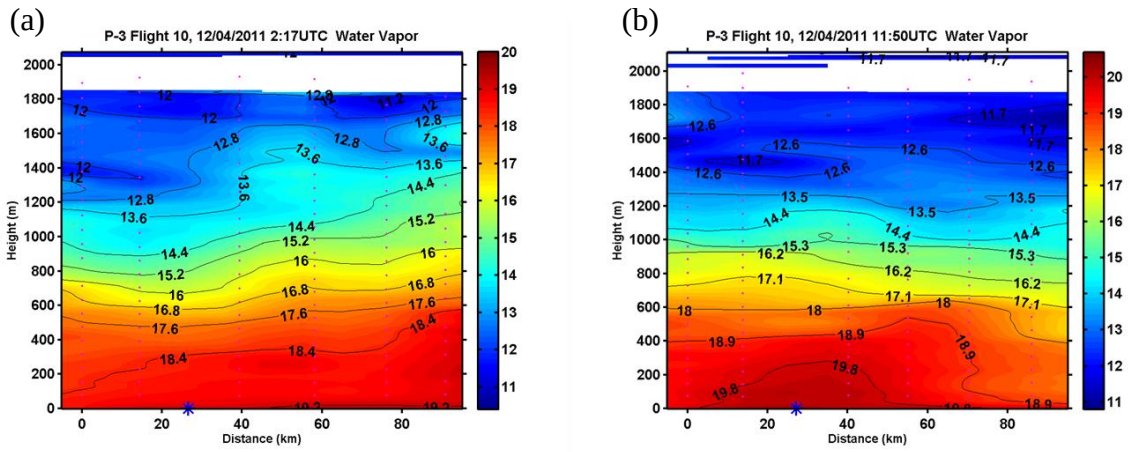

Figure 25. Same as in Fig. 24, except for specific humidity.

Although Figs. 24 and 25 are beneficial in revealing the overall modification of the low-level profiles by Diego Garcia, some of the details of the up/down-stream development of the low level wind and thermodynamic profiles cannot be seen due to the coarse vertical resolution from interpolation. Figures 26 and 27 show the individual vertical profiles from each dropsonde measurements using the original vertical resolution of about 6 m. The six panels in Fig. 26 show the progressive development of the low-level moisture between 27 km upwind and ~60 km downwind. However, the last profile, ~60 km downwind, has significantly more water vapor to a much greater depth than all the previous five profiles. It is probable that this profile represents a precipitation event and is not characteristic of Diego Garcia's island effect. Figure 28 is a plot of all the specific humidity profiles together for easy quantitative comparison. It is seen in the morning profiles (Fig. 28a) that the two downwind profiles (12 m and 31 km) show slight moisture increase compared to soundings upwind or further away downwind (49 km downwind). The soundings labeled 'marine' in this figure is from the environment within 100 km of Diego Garcia. It shows a similar moisture structure to the profile 60 km downwind, both may be under the influence of deep cloud and convection.

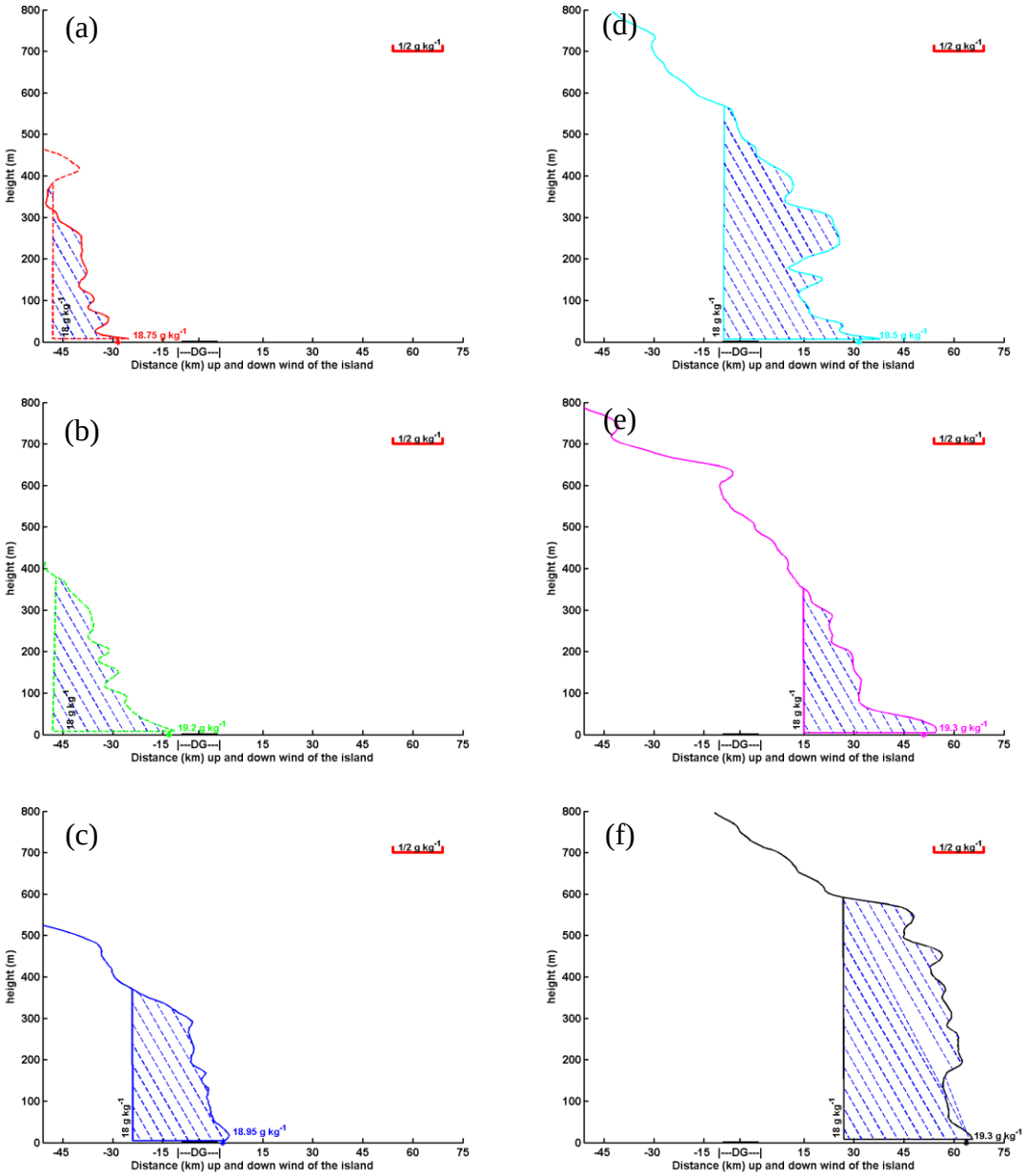

Figure 26. Specific humidity profiles from DYNAMO dropsondes launched on the **morning** of 04 December, 2011. (a) and (b) are profiles 27 km and 13 km upwind of the island respectively. (c), (d), (e), and (f) are profiles 12 km, 31 km, 49 km, and 60 km downwind of the island respectively. A reference line at 18 g kg^{-1} is given in all profiles to highlight the magnitude of moisture in the profile.

The impact of Diego Garcia on the moisture profiles are much more apparent in the afternoon soundings shown in Fig. 28b. Here, one can seen two groups of profiles,

one with lower moisture of about 19.4 g kg^{-1}, one with higher moisture of about 20 g kg^{-1}. The high moisture group is from 14 km upwind and 12 and 27 km downwind, while 28 km upwind and 42 km upwind profiles show similar water vapor content to the two profiles in the marine environment. Clearly, the presence of Diego Garcia modifies the moisture profiles within 14 km upwind and 27 km downwind, but does not exceed 28 km upwind or 42 km downwind. The more significant impact in the afternoon hours has to do with both the increased surface temperature of the lagoon and the heating of the land strip that enhanced surface moisture flux and turbulence mixing within the island plume.

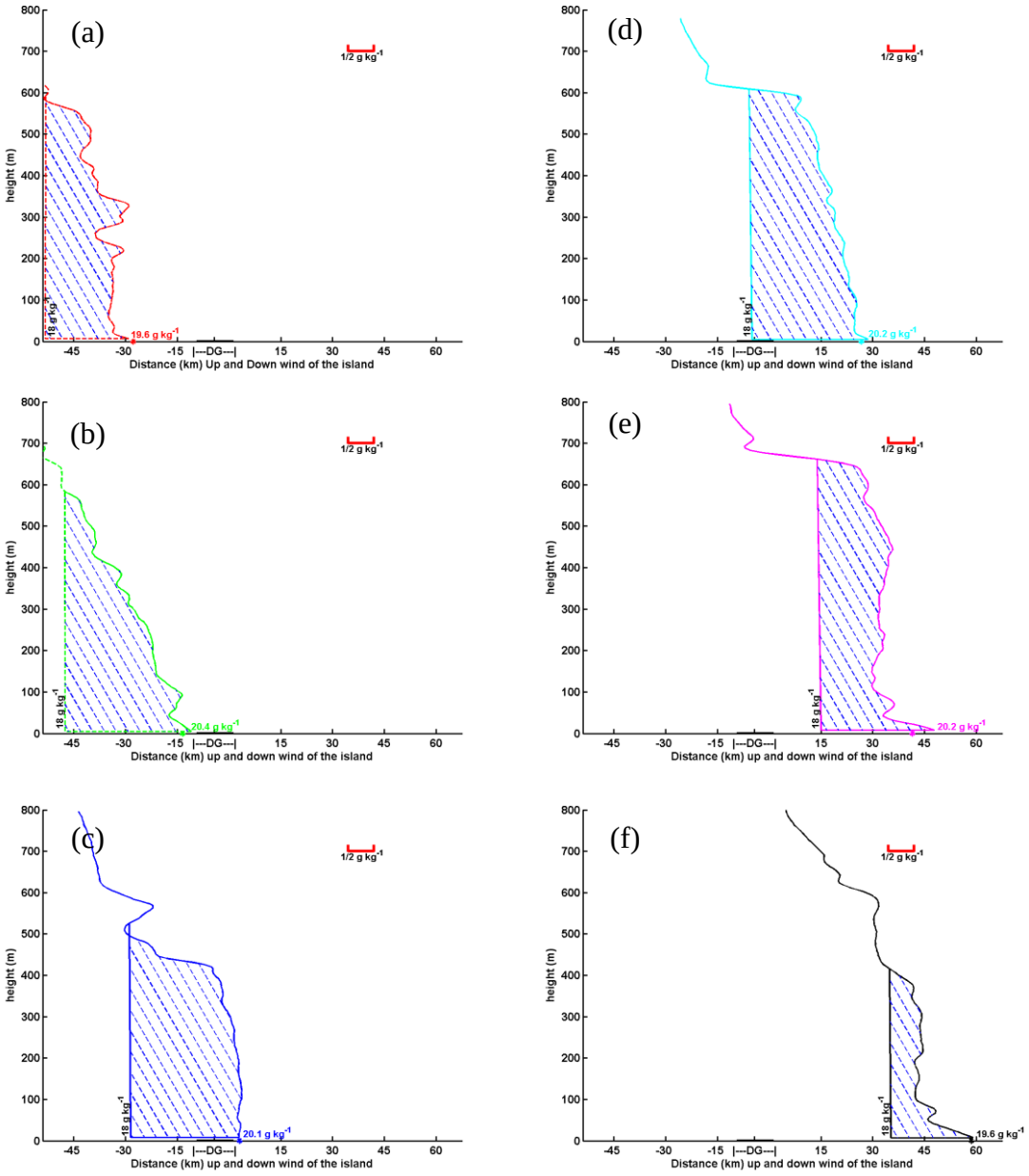

Figure 27. Same as Fig. 25 but for the afternoon of 04 December.

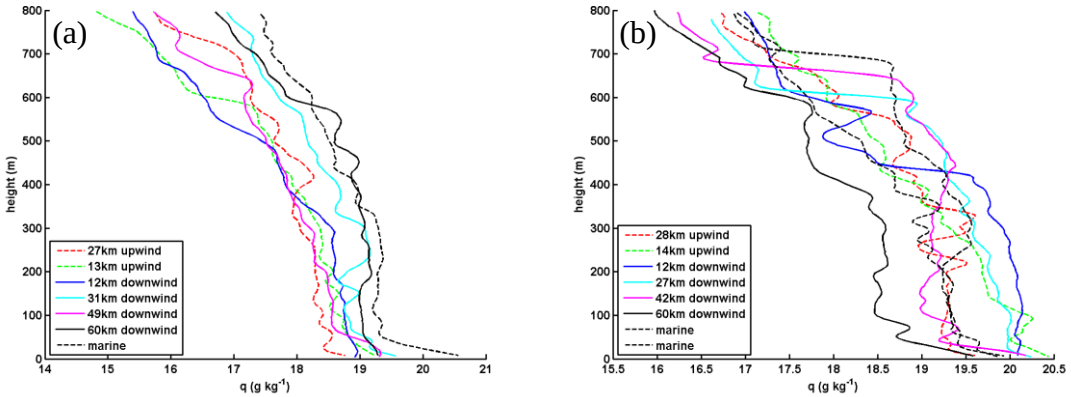

Figure 28. Low level moisture profiles for the (a) morning and (b) afternoon of 04 December, 2012. Locations of the dropsondes relative to the island are given in the legend. The profiles labeled marine are from drops away from the Diego Garcia and are taken to represent the marine environment

V. COAMPS SIMULATION OF ISLAND EFFECTS

A. OVERVIEW OF COAMPS SIMULATIONS

The Coupled Ocean and Atmospheric Mesoscale Prediction System (COAMPS®) is the US Navy's operational mesoscale forecast model. COAMPS is fully-compressible primitive-equation atmospheric model which is solved on a staggered Arakawa C grid. Due to the extremely small scale resolution of COAMPS and its mesoscale purposes it is non-hydrostatic. Operational uses of the model have used horizontal resolution as small as 0.5 km. The vertical coordinate system is sigma-z. The Navy Operational Global Atmospheric Prediction System (NOGAPS) supplies the boundary conditions used by COAMPS.

COAMPS simulations were made in the vicinity of Diego Garcia to identify the model's capability in depicting the effect of the small atoll island and its lagoon on the MBL. Five nests (Fig. 29) were used with increasing resolution starting with 40.5 km in an area centered on Diego Garcia and approximately 30°×30° in latitude and longitude. Subsequent nests were of 13.5 km, 4.5 km, 1.5 km, and 0.5 km resolution. Of note, Diego Garcia and the lagoon is not large enough to be resolved in the first three nests and is only partially resolved in nest four. Nest five does fully resolve Diego Garcia and the lagoon and has 205×205 grid points in a 1°×1° box at 0.5 km resolution. The vertical discretization for each nest was up to 30,000 m and consisted of 60 levels with the majority of those levels below 5,000 m and 24 levels below 1,250 m. The model was cold started from 00z on 02 December, 2011 with 12-hr updates and conventional meteorological data and ocean data assimilation performed. The dropsonde data from the DYNAMO field project was not included in the data assimilation dataset.

Four simulations were made for the purpose of this study: a control run with the full model (control), the full model with Diego Garcia removed from the land surface data (no-DG); a dry island run with Diego Garcia but without the moisture processes (Dry), and a model run without either Diego Garcia or moisture processes (no-DG/Dry). The Dry simulations were made with the cumulus parameterization and moist process

turned off. However, by default, cumulus parameterization is not performed in COAMPS when the grid resolution is less than 10 km. Therefore, for nests 3, 4, and 5, the Dry runs essentially had the microphysical process turned off.

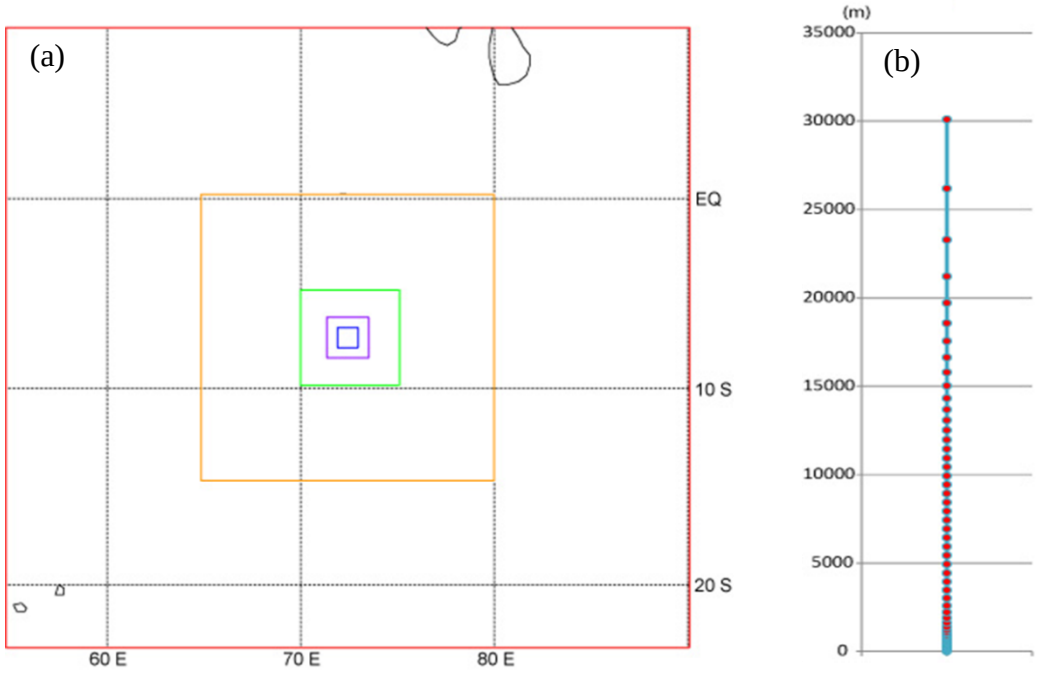

Figure 29. (a) The five COAMPS nests centered over Diego Garcia; (b) the vertical levels setup in COAMPS simulations for this work.

B. WIND EFFECTS FROM DIEGO GARCIA

The effects of Diego Garcia on the wind field are shown by the differences between two pairs of simulations: the Control and No-DG simulations, and the Dry and no-DG/Dry simulations, shown in Figs. 30 and 31. The difference between the Control and No-DG simulations reveals the island effect with full model physics. Because of the small domain size of nest 5, development of convection at scales greater than 50 km cannot be realistically represented in this domain. Therefore, the simulations with full moisture physics in the Control and No-DG runs are likely affected by the unrealistic convective field. As a result, the island effects when averaged over the lowest 500 m cannot be clearly identified (Fig. 30a). However, the island effect in wind reduction near

the surface is apparent in the simulated difference shown in Fig. 31a. The largest reduction is seen over the island with a magnitude of about 2 m s^{-1}.

The two simulations without moisture physics were designed to isolate the effects of the island only (Figs. 30b and 31b). The wind reductions downwind of Diego Garcia are clearly seen in the mean wind speed as well as in the 10-m wind in both figures. The effect of the island can be seen ~60 km downwind, although the significant modifications are seen ~20 km downwind. These results are consistent with the findings from dropsonde measurements discussed in the previous chapter.

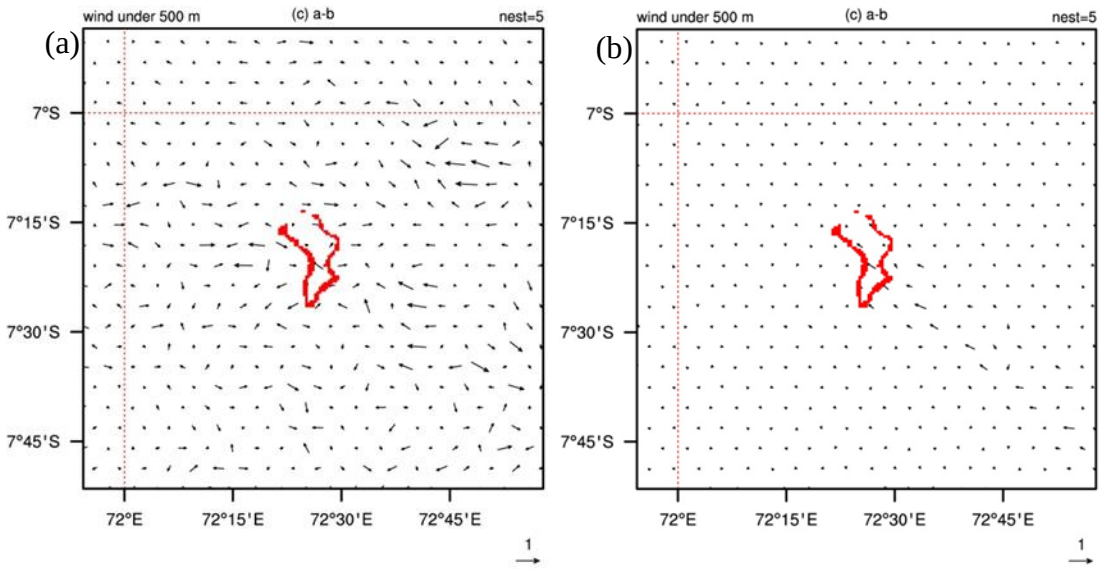

Figure 30. Differences in mean wind speed of the lowest 500 m from the inner-most domain of COAMPS simulations between (a) no-DG/Dry and Dry simulations; (b) No-DG and Control simulations. The results shown are the analyses field at 00 UTC on 04 December, 2011. The horizontal arrow at the lower-right corner denotes the magnitude of the wind vector at 1 m s^{-1}.

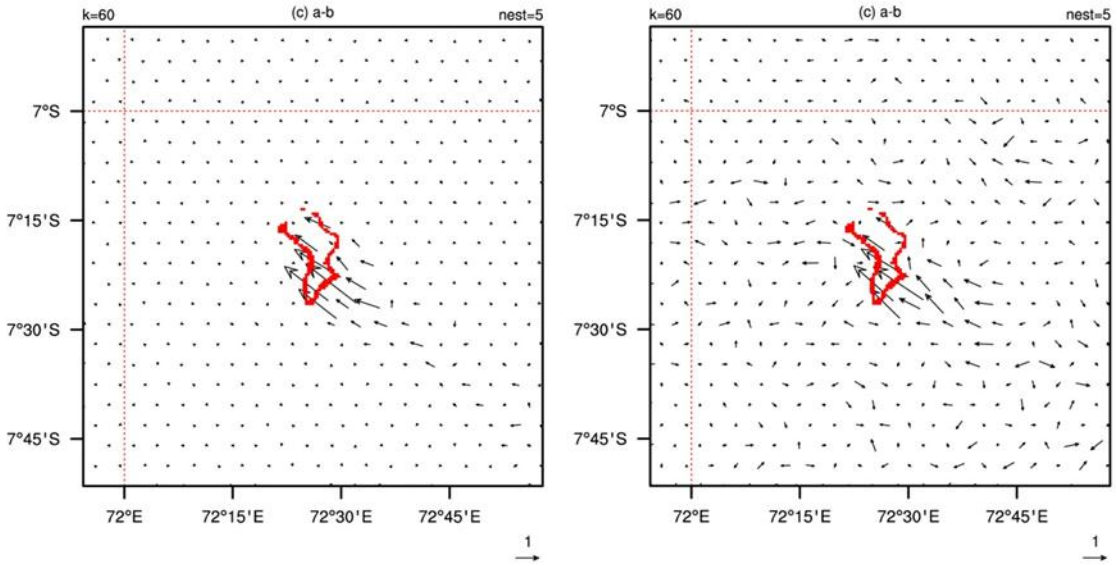

Figure 31. Same as in Fig. 29, except for 10 m wind.

C. MOISTURE EFFECTS FROM DIEGO GARCIA

The wind effects from the presence of Diego Garcia were expected and COAMPS was able to capture the downwind wind reduction. However, the moisture effects are unique with Diego Garcia and its lagoon and COAMPS simulations are not expected to represent the moisture enhancement seen from the dropsonde data. The major reason that COAMPS was unable to model the low-level moisture increase was due to the model's inability to resolve the preferential diurnal heating of the lagoon in what was characterized previously as the water island. Figure 32 displays the ground temperature control over 12 hours starting at 00z on 04 December 2011. The diurnal variation of the ground temperature of the land strip can be well represented. However, the stand-alone COAMPS cannot represent the diurnal heating of the shallow lagoon because the SST was only updated every 12 hours and there were no measurements in the lagoon. It was discussed in the previous chapter that the main cause of moisture enhancement over the island was the additional evaporation from the heated lagoon in the afternoon.

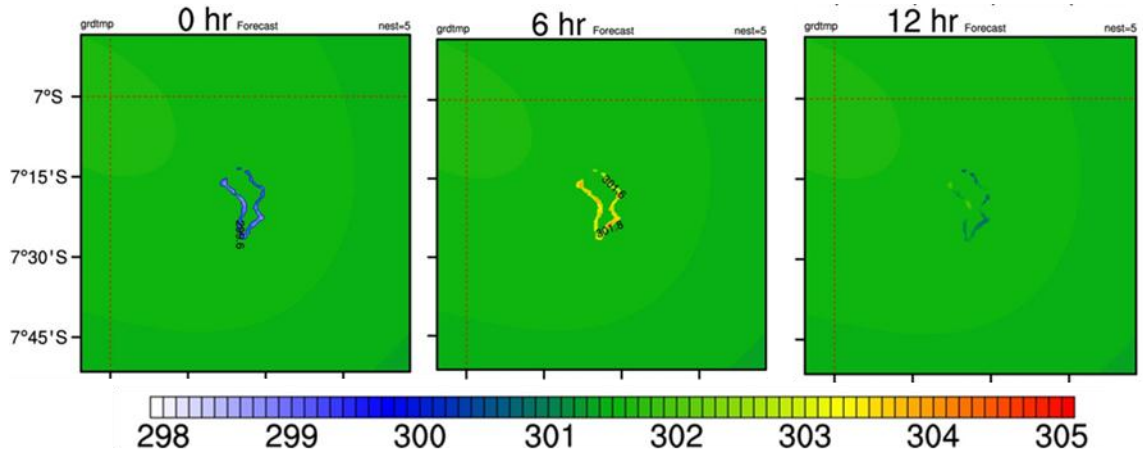

Figure 32. Ground temperature control from 00z to 12z.

THIS PAGE INTENTIONALLY LEFT BLANK

VI. REPRESENTATION OF UPSONDE FROM DIEGO GARCIA FOR MARITIME ENVIRONMENT

While it is desirable to use the rawinsonde measurements from Diego Garcia to represent the greater marine environment, the upsonde profiles need to be used with caution due to the modification of the island landmass on the lower atmosphere as demonstrated by Matthews et al. (2007) and McFarlane (2004). Because of the unique features of the different islands, their effects can vary significantly, thus it is a challenge to make corrections for the island effects.

The measurements of the island effect study on Diego Garcia on 04 December 2012 were coordinated with ground-based rawinsonde measurements. A comparison of the dropsonde and the rawinsonde measurements are shown in Figs. 33 to 35 for specific humidity, wind speed, and potential temperature, respectively. The morning sounding for specific humidity have higher surface water vapor than the marine environment by 1 to 2 g kg^{-1}. This difference will persist up to 150 m above the surface or until the balloon was out of the island plume, which measured the marine environment. In the afternoon, the balloon sounding seemed to track the island plume until ~250 m height, and sampled much larger specific humidity than any dropsonde in the marine environment. It is likely that this particular rawinsonde went through a convective cloud near Diego Garcia while the dropsondes in the marine environment were in the non-convective region. From many dropsonde measurements in DYNAMO, we have found significant spatial variability in moisture on days with convective activities.

The comparison of the island based wind measurements with those from the series of dropsondes at different upwind/downwind distances shows clearly the wind reduction over the island. In the morning soundings (Fig. 33a), two profiles showing wind reduction are the rawindsonde from the island and the dropsonde at 12 km downwind. The island-based wind profile saw a reduction layer up to about 150 m above the surface with significant low-level wind shear. At 12 km downwind, the wind shear is reduced somewhat from the island while the layer of wind reduction is deeper, to ~250 m above surface. In the afternoon soundings, all three soundings in the vicinity of the island (over

the island, 14 km upwind, and 12 km downwind) show clear signs of wind reduction up to about 200 m above the surface with the island sounding depicting a slightly shallower layer of significant wind reduction. As discussed in Chapter V, the wind reduction upwind is confined to the lowest 200 m, while that downwind extended much higher, up to about 600 m. The island sounding shows the weakest wind of all soundings, which seems to be consistent with the reduction layer from the rest of the downwind soundings extending to 42 km downwind.

The potential temperature profiles from all soundings show significant spatial variability in the vicinity of Diego Garcia. The consistency among all soundings is in the vertical gradient of the potential temperature profiles, with the exception of the sounding made from the island by rawinsonde. In the morning hours, the upsonde potential temperatures indicate a strongly stable thermal stratification up to about 150 m above the surface. In the afternoon, extremely unstable stratification was observed in the lowest 50 m above the island by the balloon sounding. It is not clear, though, whether the layer above was affected by the island due to the substantial spatial variability seen from the upwind, downwind and marine environment.

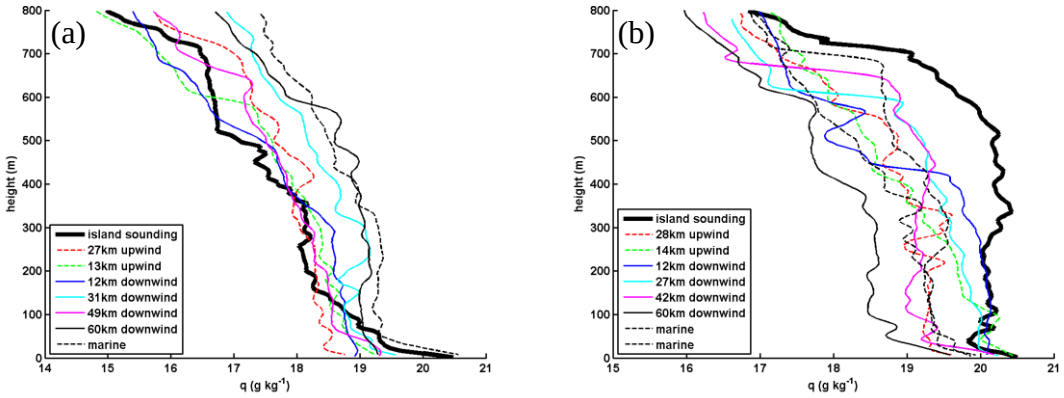

Figure 33. Specific humidity profiles of dropsondes and the island-based rawinsonde (thick black line) measurements on 04 December, 2011. Locations of the dropsondes relative to the island are given in the legend. (a) and (b) show the morning and afternoon soundings, respectively.

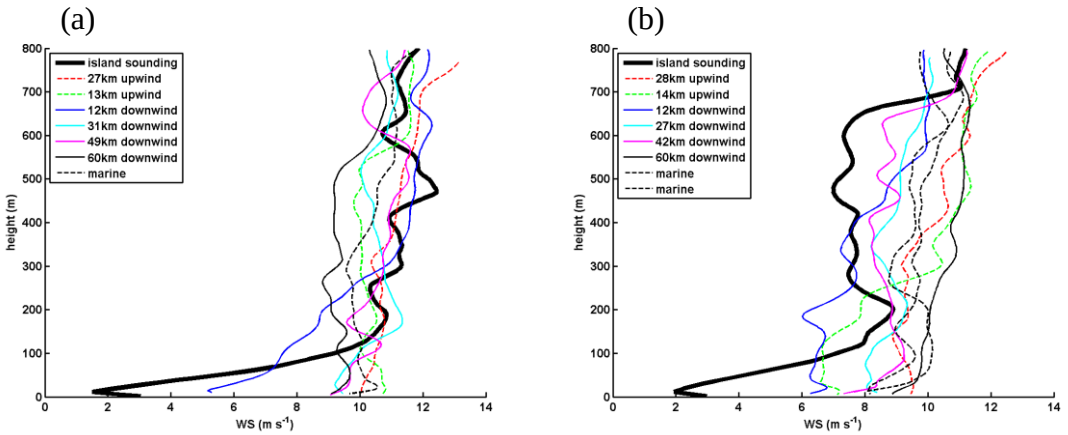

Figure 34. Same as in Fig. 32, except for wind speed.

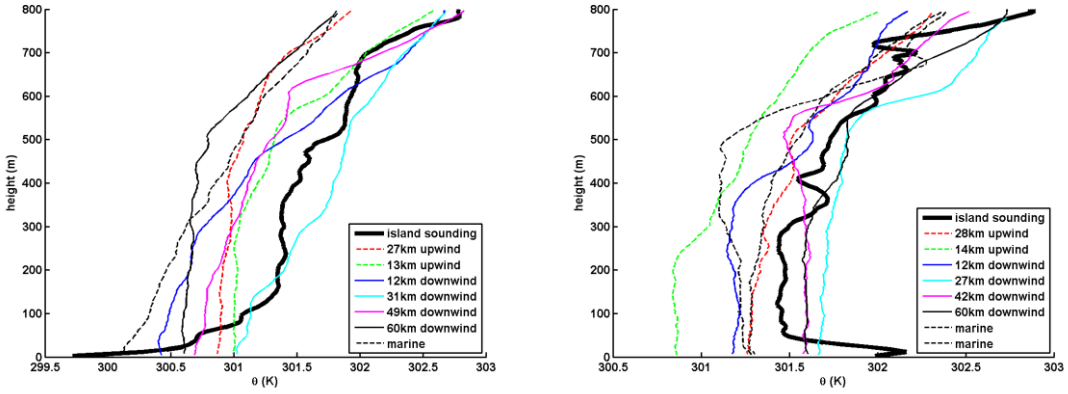

Figure 35. Same as in Fig. 32, except for potential temperature.

THIS PAGE INTENTIONALLY LEFT BLANK

VII. SUMMARY, CONCLUSIONS, AND RECOMMENDATIONS FOR FUTURE IMPLEMENTATION

A. SUMMARY AND CONCLUSION

The presence of Diego Garcia in the tropical southern Indian Ocean creates a distinctive effect on the MBL. While typical island effects and surface layer dynamics were observed in the wind field characteristics upwind, downwind, and in the greater DYNAMO field project domain, moisture effects from the preferential diurnal heating of Diego Garcia's lagoon was unique. The lagoon's diurnal SST heating as compared to the open ocean surrounding Diego Garcia is on the order of 1 to 2°C. The wind field upwind and downwind of Diego Garcia is reduced and this can be felt approximately 10 km upwind, 20 km downwind, and 200 m vertically in the morning. The range of the wind effects increase during the day and the island effect of a reduced layer of wind extended to 20 km upwind, 50 km downwind, and up to 600 m vertically in the afternoon. The magnitude of the wind speed reduction was not much different than in the morning as compared to the afternoon but the ranges were greatly increased. The moisture increase from the water island that is Diego Garcia's lagoon is due to solar heating of the top layer of the lagoon during the day. It was found that Diego Garcia's island effect is minimal in the morning regarding water vapor. In the afternoon, however, Diego Garcia's lagoon put a considerable amount of water vapor into the lower atmosphere that was mixed higher downwind. The specific humidity increase due to Diego Garcia was on the order of 0.75 to 1.5 g kg^{-1} higher than the marine environment away from the island and lagoon. In the afternoon the specific humidity from Diego Garcia affects the atmosphere in similar upwind and downwind ranges, but extends lower to approximately 500 m vertically. COAMPS modeling of the effect Diego Garcia has on the MBL captured the wind reduction in the inner-most domain only with a grid resolution of 500 m. Attempts to model the moisture effects from Diego Garcia was unsuccessful due to the multi-scale moisture processes introduced by tropical convections and the limited coverage of the simulation domain in order to define the footprint of the small island.

The effects of the Diego Garcia atoll are found to be different from all other islands discussed in previous studies. With Hawaii's big island, the predominate effect is seen in modifications of TC intensity and track due to the flow blocking, wind shadow, and other large synoptic scale interaction with the island's outstanding topography. Nauru is a small island with little relief but the significant contrast in surface properties contribute to roughness change and diurnal heating, which has profound impacts on the boundary layer. The combination of modifications to temperature and specific humidity by Nauru produced a cloud street in the tropical environment that can exist up to 120 km downwind of the island. For Diego Garcia the low relief and presence of the lagoon lead to the predominate boundary layer modification of moisture plumes in the lower levels up and downwind of the island. It is possible that such changes in the low-level thermodynamics can lead to downstream cloud formation. However, extensive clouds associated with the island effects have not been identified during the DYNAMO field measurement period.

B. RECOMMENDATIONS

The study of the effects of Diego Garcia in modifying the marine environment provides the foundation of evaluating the data quality of the island-based measurements in representing the MJO development. To help better quantify this issue, future research can benefit from more accurate measurements of the diurnal heating of Diego Garcia's lagoon as compared to the neighboring ocean and tracking the moisture plumes to determine if the increase water vapor has an effect on precipitation or clouds streets downwind. More cases with the island effect foci should also validate conclusions from this thesis research.

LIST OF REFERENCES

Amante, C. and B. W. Eakins, 2009: ETOPO1 1 Arc-minute Global Relief Model: Procedures, Data Sources and Analysis. NOAA Technical Memorandum NESDIS NGDC-24, 19.

Arnfeld, A., 2002: Two Decades of Urban Climate Research: a review of turbulence, exchanges of energy and water, and the urban heat island, *J. of Climatology*, **23**(1), 1-26.

Balling, R. and R. Cerveny, 1987: Long-term associations between wind speeds and the urban heat island of Phoenix, Arizona, *J. Clim. Appl. Meteor.*, **26, 712-716.**

Chambers, C. and T. Li, 2011: The effect of Hawaii's big island on track and structure of tropical cyclones passing to the south and west, *Amer. Meteor. Soc.*, **139**, 3609-3627.

Changnon, S. (Ed.), 1981: *METROMEX: A Review and Summary*. Meteor Monographs, 18(40). Amer. Meteor. Soc. Boston. 181pp.

Claussen, M., 1987: The flow in a turbulent boundary layer upstream of a change in surface roughness. *Bound.-Layer Meteor*., **40**, 31-86.

Commander Naval Meteorology and Oceanography Command, 2002: Local area forecaster's handbook for Diego Garcia, *Navcentmetocdetdginst 3140.2*, 1-37.

Draxler, R., 1986: Simulated and observed influence of the nocturnal urban heat island on the local wind field. *J. Clim. Appl. Meteor.*, **25**, 1125-1133.

Erickson, A., W. Ladwig, and J. Mikolay, 2010: Diego Garcia and the United States' emerging Indian Ocean strategy, *Asian Security*, **6**. no. 3, pp. 214-37.

Hock, T., and J. Franklin, 1999: The NCAR GPS dropwindsonde, *Bulit. Amer. Meteor. Soc.*, **80(3)**, 407-420.

Katsoulis, B. and G. Theoharatos, 1985: Indications of the urban heat island in Athens, Greece. *J. Clim. Appl. Meteor.*, **24**, 1296-1302.

Kim, H., 1992: Urban heat island, *Int. J. Remote Sensing*, **13**(12), 2319-2336.

Long, C. and S. McFarlane, 2011: Quantification of the impact of Nauru island on the ARM measurements, *J Applied Meteor. And Climatology*, **51**, 628-636.

Matthews, S., J. Hacker, J. Cole, J. Hare, C. Long, and R. Reynolds, 2007: Modification of the atmospheric boundary layer by a small island: observations from Nauru, *Amer. Meteor. Soc.*, **135**, 891-905.

McFarlane, S., C. Long, and D. Flynn, 2004: Impact of island-induced clouds on surface measurements: analysis of the ARM Nauru island effect study data, *Amer. Meteor. Soc.*, **44**, 1045-1065.

Mitsuta, Y., N. Monji, and D. Lenschow, 1986: Comparisons of aircraft and tower measurements around Tamara island during AMTEX '75. *J. Clim. Appl. Metoer.*, **25**, 1946-1955.

Monin, A.S. and A. Obukhov, 1954: Basic laws of turbulent mixing in the surface layer of the atmosphere.". *Tr. Akad. Nauk SSSR Geofiz. Inst* **24**: 163–187.

Mook, F. van, 2002: Driving rain on building envelopes, *Bouwstenen series of the Faculty of Architecture*, **69**.

Oke, T., 1982: The energetic basis of the urban heat island. *Quart J. Roy. Meteor. Soc.*, **108**, 1-24.

Sass, R., 2012: It's not cool to be hot in Houston. Self-published online. Last accessed August 2, 2012, at http://www.ruf.rice.edu/~sass/UHI.html.

Stoddart, D. and J. Taylor, 1971: Geography and ecology of Diego Garcia atoll, Chagos archipelago, *The Smithsonian Inst.,* retrieved from http://www.sil.si.edu/digital collections/atollresearchbulletin/issues/00149x.pdf. Last accessed June 19, 2012.

Stull, R. B., 1988: *An Introduction to Boundary Layer Meteorology*. Kluwer Academic Publishers, 670 pp.

U.S. Navy Support Facility Diego Garcia, 2005: Diego Garcia integrated natural resources management plan, *Govt. Doc.*, retrieved from http://www.zianet.com/ tedmorris/dg/2005NRMP.pdf. Last accessed June 19, 2012.

Wang, J., 2005: Evaluation of the dropsonde humidity sensor using data from DYCOMS-II and IHOP_2002. *Amer. Meteor Soc.*, **22**, 247-257.

Zhang, C., S. Rutledge, R. Johnson, and R. Houze 2011: Experiment design overview (EDO) dynamics of the MJO (DYNAMO).

INITIAL DISTRIBUTION LIST

1. Defense Technical Information Center
   Ft. Belvoir, Virginia

2. Dudley Knox Library
   Naval Postgraduate School
   Monterey, California

3. Professor Qing Wang
   Department of Meteorology
   Naval Postgraduate School
   Monterey, California

4. Professor Wendell A. Nuss
   Department of Meteorology
   Naval Postgraduate School
   Monterey, California